ADVANCED RTG AND THERMOELECTRIC MATERIALS STUDY

November, 1971

Final Report for Period January-October, 1971

Contract NAS5-11394

Prepared for

GODDARD SPACE FLIGHT CENTER
Greenbelt, Maryland 20771

Philip E. Eggers

BATTELLE
Columbus Laboratories
505 King Avenue
Columbus, Ohio 43201

1. Report No.	2. Government Accession No.	3. Recipient's Catalog No.
4. Title and Subtitle Advanced RTG and Thermoelectric Materials Study		5. Report Date November, 1971
		6. Performing Organization Code BCL
7. Author(s) Philip E. Eggers		8. Performing Organization Report No.
9. Performing Organization Name and Address BATTELLE Columbus Laboratories 505 King Avenue Columbus, Ohio 43201		10. Work Unit No.
		11. Contract or Grant No. NAS5-11394
12. Sponsoring Agency Name and Address National Aeronautics and Space Administration Goddard Space Flight Center Greenbelt, Maryland		13. Type of Report and Period Covered Type III Final Report January 1971 to October 1971
		14. Sponsoring Agency Code 716
15. Supplementary Notes		

16. Abstract

A comprehensive, generalized two-dimensional RTG analysis computer program has been developed. This program is capable of analyzing any specified RTG design under a wide range of transient as well as steady-state operating conditions.

The feasibility of a new concept for the design of segmented (or single-phase) thermoelectric couples has been demonstrated. In the present study, a SiGe-PbTe segmented couple involving pressure contacted junctions at the intermediate- and hot-junction temperatures was successfully encapsulated in a hermetically sealed bellows enclosure. This bellows-encapsulated couple was operated between a hot- and cold-junction temperature of 1200 K and 450 K, respectively, with a measured energy-conversion efficiency of 7.6 $\pm$ .5 percent.

An experimental study of selected sublimation barrier schemes revealed that a significant reduction in the sublimation rate of p-type PbTe could be achieved by using multiple layers of SiO_2 fibers. A comparison of the "barrier effectiveness" is given for three different barrier designs.

17. Key Words (Selected by Author(s))	18. Distribution Statement
Thermoelectric Energy Conversion Segmented SiGe-PbTe Couples Transient RTG Analysis Sublimation Barriers	

19. Security Classif. (of this report)	20. Security Classif. (of this page)	21. No. of Pages	22. Price*
Unclassified	Unclassified	86	

PREFACE

Task I. Development of Computer Program for the Transient Analysis of Radioisotope Thermoelectric Generators

Objective

The overall objective of this task is to modify the existing generalized Space Generator Computer Program (GESPGN) to provide the capability for predicting the output power and temperature profile of an RTG in the presence of time-dependent operating conditions.

Scope of Work

The transient analysis of an arbitrary RTG design has been developed within the framework of the RTG weight optimization computer program GESPGN, which had been developed previously under NAS5-9160 and NAS5-10497. This major revision of the existing computer program enables the analyst to predict the performance of an RTG in both the transient and steady-state operating modes. A total of eight "transients" have been included in the revised computer program (renamed TRANRTG) since they are generally accepted as the principal effects which influence the long- and short-term performance characteristics of RTG's. The transients accommodated by the TRANRTG computer program include:

1. Cold start of RTG during insertion of radioisotope heat source
2. Changing boundary conditions during simulated launch of RTG.
3. Solar flux and/or planetary albedo variations
4. Thermopile degradation
5. Thermal insulation degradation
6. Electrical load fluctuations
7. Surface emittance changes in the radiator heat sink due to micrometeorite damage, etc.
8. Heat source power degradation as a result of radioisotope decay

Conclusions

A comprehensive RTG computer program (TRANRTG) has been successfully developed providing capabilities heretofore unavailable to the RTG analyst. Specifically, the TRANRTG program enables the analyst to optimize the design of an RTG with respect to weight as well as study the effect of specified long- and short-term transients on the RTG's thermal and electrical operating characteristics. This transient analysis computer program is well suited to aid the analyst in either (1) the design and evaluation of future RTG configurations or (2) evaluation of existing RTG designs. For example, the TRANRTG computer program could be used in performing simulation studies involving existing RTG designs such as the SNAP-19. Consequently, with this program, hypothesized RTG degradation mechanisms can be modeled and studied and finally compared with available empirically derived degradation characteristics.

The 2-D TRANRTG computer program developed in this task provides a comprehensive RTG analysis capability. The analyst need only specify materials properties, RTG design requirements, and transient operating conditions. Hence, the application of the TRANRTG program to RTG design and analysis will (1) enhance the understanding of the relative importance various transients on RTG performance, (2) permit RTGs to be optimized more comprehensively than before with respect to both weight and performance stability in the presence of the anticipated transients, and (3) enhance the value of present RTG experimental data (both radioisotope fueled and electrically heated) since these data can be used in conjunction with comprehensive degradation models.

Summary of Recommendations

The results of preliminary checkout runs of the TRANRTG computer program indicate that several analytical studies would be meaningful at this point in the development and qualification of RTG's for present and future missions. First, an analytical study involving presently existing RTG designs (e.g., the SNAP-19 RTG) would permit presently proposed degradation models to be studied and compared with available thermoelectric generator experimental data. For example, degradation phenomena such as erosion of thermoelements with subsequent RTG "thermal runaway" could be readily studied. Second, an analytical study involving future RTG designs (e.g., the multi-hundred-watt RTG) would permit the final design optimization to include factors such as the response of the RTG to the anticipated transient operating conditions. Third, the present computer program could be effectively applied to study transient RTG behavior during launch.

Task II. Fabrication and Performance Testing of SiGe-PbTe Segmented Thermoelectric Generators

Objective

The overall objective of this task is to fabricate segmented SiGe-PbTe segmented couples, perform extended life tests, and measure conversion efficiency.

Scope of Work

The technology used in the fabrication of the SiGe-PbTe couples was drawn from the NASA-Goddard contract, NAS5-21099. These segmented couples were operated in vacuum and incorporate pressure contacted PbTe/W intermediate junctions and SiGe/C hot junctions. The life testing and efficiency measurements were a continuation of evaluative studies initiated for this couple concept under NASA-Goddard contract NAS5-21099. The experimental work performed under this task included:

1. Life testing of SiGe-PbTe segmented couples in the "constant thermal input" test fixture developed previously.

2. Incorporation of selected segmented couple design changes offering improved output power stability, e.g., the utilization of hermetically sealed bellows enclosures.

Conclusions

A new approach to the design of SiGe-PbTe segmented thermoelectric couples, involving hermetically sealed bellows enclosures and pressure-contacted junctions, has been successfully demonstrated. The results of these preliminary studies indicate the feasibility of eliminating the use of conventional spring-loading hardware normally required for thermoelectric converters involving pressure-contacted junctions. The elimination of this conventional approach to providing axial spring-loading pressure is significant as the "spring and follower" has been the source of significant thermal impedances (30 to 50 C difference) between the thermoelectric element and the radiator. In addition, the "spring and follower" design has frequently failed due to seizing at the follower/radiator cold frame interface with subsequent loss of the needed axial loading pressure.

In the present design, Inconel 718 bellows provide a hermetic enclosure for the thermoelectric sleeves as well as the axial loading required to effect low electrical-junction resistances. In addition, the incorporation of pressure-contacted junctions eliminate the need for the complicated transition materials usually required at the interface of materials possessing greatly differing thermal expansivities. The present design involves pressure-contacted junctions at both the SiGe/PbTe interface and the SiGe/C hot-strap interface. Although the use of pressure-contacted junctions at the SiGe hot-strap interface simplify the overall design of the segmented couple, they also are a potential source of high junction resistance.

The results of preliminary evaluation studies indicate that the "bellows-encapsulated" SiGe-PbTe segmented element concept provides (1) a hermetically sealed enclosure which isolates the thermoelectric element from its environment (typically involving fibrous insulations or metallic foils operating in vacuum), (2) a scheme for providing adequate axial spring-load pressure to effect low junction resistances, (3) a scheme for the "cantilever support" of the thermoelectric elements from the cold frame of the heat sink, and (4) a scheme for operating the thermoelectric elements with internal* cover-gas pressures of up to 75 psia while operating the thermopile in air, vacuum, or other typical RTG operating environments.

The results of theoretical analyses indicate that the present "bellows-encapsulated" SiGe-PbTe segmented couple design offers a conversion efficiency of 7.97 percent**. This calculation includes 11 percent by-pass heat loss in the 4.5-mil-thick Inconel 718 bellows. The results of preliminary conversion efficiency tests yielded a measured couple efficiency of 7.65 percent. This value is 10-20 percent higher than that reported*** for SiGe alone operating at the same temperatures. Hence, these results support the predicted improvement in conversion efficiency expected for "segmented" SiGe-PbTe couples.

The life testing of the "bellows-encapsulated" SiGe-PbTe segmented couples was limited by present inadequacies in the design of the hot-strap/hot-shoe/SiGe junctions. Hence, in the absence of experimental results, no conclusions can be formed regarding the stability of the output power and efficiency of this segmented couple concept. However, the present approach to thermoelectric couple design potentially offers an ideal condition for operating thermoelectric elements. Specifically, the hermetically sealed bellows enclosure allows the thermoelectric element to be operated independently of the thermopile environment which is generally the principal source for gaseous contamination (outgassing of thermal insulation) and/or evaporative erosion (vacuum environments).

---

* within the hermetically sealed bellows

** operating at cold and hot junction temperatures of 175 C and 900 C, respectively

*** "Silicon Germanium Materials and Module Development Program", Electronics Components Division of RCA, AEC contract AT(29-2)-2510.

Summary of Recommendations

The results of preliminary experimental studies involving the bellows-encapsulated SiGe-PbTe segmented couple indicate a need for additional developmental efforts in the areas of the SiGe/hot-shoe/hot-strap junctions. All other aspects of the present concept proved successful during the preliminary proof-of-concept experiments.

A supplementary effort is recommended for the extension of the bellows-encapsulated concept to thermopile designs involving a single stage thermoelement such as the oxygen-sensitive 2p PbTe and 3p PbSnTe materials and the relatively volatile TAGS-85 thermoelectric alloy.

Task III. Study of Sublimation Barriers for Vacuum Operation of Thermoelectric Elements

Objective

The overall objective of this task is to study the relative effectiveness of selected materials and techniques in suppressing sublimation of thermoelectric materials in vacuum environment.

Scope of Work

The effect of a mechanical barrier, e.g., a mica sleeve surrounding a thermoelement in reducing the rate of sublimation at the hot junction was disclosed in a preliminary study by J. W. Killian of NSRDC.* A more comprehensive study has been undertaken in this task in order to determine the effectiveness of selected "packing" materials and "barrier" techniques in the suppression of sublimation of thermoelectric materials operating in vacuum. The experiments involved ingradient operation of the thermoelectric element in small-volume systems with selected packing materials and barrier techniques applied. The effectiveness of the sublimation barrier technique was experimentally evaluated by (1) weight-loss measurements, (2) observation of dimensional changes of thermoelectric elements, and (3) posttest Seebeck coefficient traverse measurements.

Both thermal insulating materials (e.g., microquartz fibers) and mica sleeving were evaluated in this study in order to assess their barrier effectiveness.

*Killian, J. W., "Method to Arrest Weight Loss of PbTe at Elevated Temperatures in Vacuum", 3rd Intersociety Energy Conversion Engineering Conference Proceedings, August, 1968, p. 272.

Conclusions

An effective sublimation barrier scheme has been identified which permits stable operation of materials such as 2p PbTe in vacuum at hot-junction temperatures of up to ~ 535 C for extended periods. The most effective sublimation barrier scheme studied involves a shroud of close-packed oxide fibers wrapped around a mica sleeve enclosing the thermoelectric element. The results of ingradient operation of 2p PbTe in vacuum indicate a weight loss of 0.01 to 0.04 percent after ~ 450 hrs at a hot-junction temperature of 530 C. This rate of weight loss is a factor of 10 to 40 times lower than that observed for identical experiments involving a close-fitting mica sleeve. Hence, on the basis of a percent weight loss, the oxide-fiber shroud over mica sleeve barrier scheme is far superior to the other barrier schemes investigated for 2p PbTe. A more meaningful interpretation of these results is afforded by translating the observed rate of evaporative erosion of thermoelectric material (weight loss) to a rate of electrical resistance increase (due to decreased cross-sectional area in the vicinity of the hot junction). For the present experimental conditions, the 0.04 percent weight loss in ~ 450 hrs corresponds to a total element resistance increase of less than 0.2 percent in ~ 450 hrs. Hence, the present studies have identified a potential approach for operating "volatile" thermoelectric materials such as 2p PbTe for extended periods (1-3 years) with tolerably low evaporative erosion, i.e., resistance increase. Furthermore, the present sublimation barrier scheme would significantly reduce the rate of evaporative erosion of thermoelectric materials operated in inert atmospheres, e.g., the TAGS-85 materials operating in Ar/He atmospheres.

Summary of Recommendations

The encouraging results obtained in short-term (~ 450 hr), ingradient sublimation tests suggest the need for longer test periods. This need arises from the fact that the rate of evaporative erosion is not necessarily linear with time. For example, as evaporative erosion proceeds, the total peripheral surface area of the thermoelectric element in the hot-junction region decreases, the subsequent rate of evaporation tends to decrease. However, in an actual generator (neglecting the effect of radioisotope decay), the evaporative erosion causes an increase in the thermal impedance in the hot-junction region of the thermoelectric element, hence increasing the hot-junction temperature and the rate of evaporative erosion, with time. Furthermore, in the case of the oxide-fiber shroud barrier scheme, the evaporative erosion may be progressively self-inhibiting since the fiber interstices may accumulate sublimation deposits which may impede further sublimation.

Thus, the significant reductions in evaporative erosion rates observed for short test periods (~ 450 hr) should be extended to ~ 1000- and ~ 5000-hr test periods. These extended test periods will not only evaluate the present schemes for long-duration operation but will provide empirical information regarding the rate of change of the evaporate rate over extended periods. Hence, the next series of sublimation experiments would provide the data necessary to predict the adequacy of the selected barrier design for substantially greater periods of operation (20,000 hrs or more).

ACKNOWLEDGEMENTS

Significant contributions were made by Dr. John L. Ridihalgh (computer program development) and Messrs. John J. Mueller and Arnold G. Carter (design, development, and fabrication of bellows-encapsulated SiGe-PbTe segment couples). Grateful acknowledgements are also due Mr. Si Manson of NASA-Headquarters who has provided many valuable discussions during the course of this program.

TABLE OF CONTENTS

	Page
DISCUSSION	1
Task I. Development of Computer Program for the Transient Analysis of Radioisotope Thermoelectric Generators	1
Introduction	1
Development of Analytical Model	1
Input/Output	10
Task II. Fabrication and Performance Testing of SiGe-PbTe Segmented Thermoelectric Generators	12
Introduction	12
Design of Segmented Couple	13
Design of Bellows Enclosure	15
Fabrication of Bellows-Encapsulated Segmented Elements	19
Experimental Results	22
Task III. Study of Sublimation Barriers for Vacuum Operation of Thermoelectric Elements	27
Introduction	27
Development of Sublimation Barrier Schemes	27
Experimental Procedure	29
Experimental Results	32
REFERENCES	34
APPENDIX A	
USERS MANUAL FOR TRANRTG RTG TRANSIENT ANALYSIS COMPUTER PROGRAM	A-1
APPENDIX B	
SAMPLE TRANRTG OUTPUT	B-1

LIST OF TABLES

TABLE 1.	SUMMARY OF RTG TRANSIENT OPERATING CONDITIONS	2
TABLE 2.	COMPUTED DIMENSIONS AND PERFORMANCE PARAMETERS FOR SiGe-PbTe SEGMENTED COUPLES	16

LIST OF TABLES (Continued)

Page

TABLE 3. COMPUTED AND MEASURED PERFORMANCE PARAMETERS FOR BELLOWS-ENCAPSULATED SiGe-PbTe SEGMENTED COUPLES 26

TABLE 4. SUMMARY OF WEIGHT LOSS FOR 2p-PbTe ELEMENTS OPERATED IN VACUUM AND INVOLVING SELECTED SUBLIMATION BARRIER SCHEMES. 33

LIST OF ILLUSTRATIONS

FIGURE 1. TRANSIENT RTG MAIN PROGRAM FLOW CHART 4

FIGURE 2. LONGITUDINAL VIEW OF RTG SHOWING REGION TO BE INCLUDED IN HEAT-TRANSFER ANALYSIS. 7

FIGURE 3. TWO-DIMENSIONAL ANALYTICAL MODEL FOR HEAT TRANSFER ANALYSIS OF RTG DURING TRANSIENT OPERATION. 8

FIGURE 4. BELLOWS-ENCAPSULATED THERMOELECTRIC ELEMENT FOR USE IN LIFE-TEST EFFICIENCY MEASUREMENT APPARATUS 14

FIGURE 5. HEAT LOSS AS A FUNCTION OF SEGMENTED SiGe-PbTe THERMOELECTRIC ELEMENT LENGTH FOR SEVERAL BELLOWS WALL THICKNESSES AND HEAT-SINK-EXTENSION LENGTHS 18

FIGURE 6. COMPOSITE VIEW OF SEGMENTED SiGe-PbTe ELEMENT INCLUDING PbTe SEGMENT, W INTERMEDIATE SHOE, SiGe SEGMENT AND GRAPHITE HOT SHOE 20

FIGURE 7. BELLOWS-ENCAPSULATED SiGe-PbTe SEGMENTED ELEMENTS SHOWING Ni HOT STRAP AND EVALUATION/FILL TUBES. 21

FIGURE 8. BELLOWS-ENCAPSULATED SiGe-PbTe SEGMENTED ELEMENTS FOLLOWING EVACUATION, BACKFILL WITH ARGON, AND CLOSURE. . 23

FIGURE 9. LIFE-TEST AND EFFICIENCY-MEASUREMENT APPARATUS WITH SiGe-PbTe SEGMENTED ELEMENTS ATTACHED TO HEAT-FLUX TRANSDUCER/HEAT-SINK ASSEMBLY 23

FIGURE 10. LIFE-TEST AND EFFICIENCY-MEASUREMENT APPARATUS SHOWING THERMAL INSULATION AND HEAT-SOURCE/SPECIMEN/HEAT-SINK CAVITY. 23

LIST OF ILLUSTRATIONS (Continued)

Page

FIGURE 11. LIFE-TEST AND EFFICIENCY-MEASUREMENT APPRATUS WITH SPECIMEN IN PLACE (SPECIMEN INSIDE THERMAL INSULATION CAVITY IS NOT VISIBLE IN THIS PHOTOGRAPH) 24

FIGURE 12. LIFE-TEST EFFICENCY-MEASUREMENT APPARATUS. 25

FIGURE 13. BASIC SPECIMEN CONFIGURATION FOR SUBLIMATION-BARRIER STUDIES. 28

FIGURE 14. BARRIER SCHEMES FOR SUPPRESSING SUBLIMATION OF THERMOELECTRIC MATERIALS 30

FIGURE 15. AMPOULE TEST FIXTURE (REVISED DESIGN). 31

FIGURE B-1 CALCULATED RTG NORMALIZED POWER VERSUS TIME. . . . . .

DISCUSSION

Task I. Development of Computer Program for the Transient Analysis of Radioisotope Thermoelectric Generators

Introduction

The application of radioisotope thermoelectric generators (RTG's) to space electrical power requirements has been successfully demonstrated during the past 5 years. During this period, the knowledge of thermopile-degradation mechanisms has increased significantly and afforded insight into the ultimate stability of the thermoelectric components. Most of the extra-terrestrial applications (usually $\leq$ 1-year missions) of RTG's to date have involved relatively stable operating conditions with only a limited number of imposed transient operating conditions. For example, the NIMBUS RTG's in earth orbit experience transients due principally to modest changes in planetary albedo and incident solar flux. However, future missions will subject RTG's to multiple transient conditions due to (1) length of the mission (3-12 years), hence, significant changes in the thermal inventory due to radioisotope decay as well as thermopile degradation, (2) increased distance from the sun, hence incident flux decrease with time, and (3) change in radiator emittance/reflectance due to micrometeorite damage.

The present computer program* has been developed to meet the growing need for predicting the thermal and electrical operating characteristics of given RTG designs in the presence of one or several transient conditions. The following discussion discloses the complex nature of the present RTG transient analysis program. The complexities derive from the interdependencies of the thermopile performance, RTG temperature profile, thermal conductance of the thermopile, thermal inventory, and radiator boundary conditions.

Development of Analytical Model

The first step in the development of the transient RTG computer program (so called TRANRTG) involved an examination of the principal transient effects to be studied together with the affected independent and dependent variables. The results of this examination are summarized in Table 1 and reveal two significant characteristics of the selected transient effects. First, the transient effects can be subdivided into two general classes of transients, viz, the "equilibrium" and "nonequilibrium" classifications, according to the time characteristic of their source. For example, the thermal decay of typical radioisotopes used in RTG's occurs at a sufficiently low rate to assume that the RTG operates under equilibrium conditions. In this case, the analysis of the RTG can be effected by performing steady-state thermal analyses at selected time intervals using the properly adjusted thermal inventory. However, the

---

* Copies of this computer program are available from the NASA-Goddard Space Flight Center.

TABLE 1. SUMMARY OF RTG TRANSIENT OPERATING CONDITIONS

	Transient Effect	Source(s)	Independent Variable(a)	Dependent Variables	Classification of Transient
I.	Decrease in thermal inventory	. Radioisotope decay	Q_{HS}	T_{RAD}, T_c, T_H, Q_{LOSS}, P_E, $\delta P_E/\delta t$	. Equilibrium
II.	Change in radiator temperature	. Incident solar flux . Planetary albedo . Radiator surface/emittance changes	T_{RAD}	T_c, T_H Q_{LOSS}, P_E, $\delta P_E/\delta t$	. Nonequilibrium . Nonequilibrium . Equilibrium
III.	Change in Seebeck coefficient, electrical resistivity, thermal conductivity, and contact resistivity of T/E materials	. Thermopile degradation	S, ρ, k, ρ_c (n and p-leg)	T_c, T_H, T_{RAD} Q_{LOSS}, P_E, $\delta P_E/\delta t$	. Equilibrium
IV.	Change in heat losses	. Change in thermal conductivity of insulation components	k_{INS}	T_c, T_H, T_{RAD} Q_{LOSS}, P_E, $\delta P_E/\delta t$	. Equilibrium
V.	Changes in electrical load	. Variation in duty cycle	R_{LOAD}	T_c, T_H, T_{RAD} Q_{LOSS}, P_E, $\delta P_E/\delta t$	. Nonequilibrium and equilibrium
VI.	Initial startup, i.e., cold start	. "Fueling" of RTG	Q_{HS}	T_c, T_H, T_{RAD} Q_{LOSS}, P_E	. Nonequilibrium
VII.	Reduction in contact area and of T/E elements' cross-sectional area	. Sublimation of T/E materials	A_x (n- and p-leg)	T_c, T_H, T_{RAD}, Q_{LOSS} P_E, $\delta P_E/\delta t$	. Equilibrium
VIII.	Changing boundary conditions	. Launch profile of RTG	h, T_b	T_c, T_H, T_{RAD}, P_E	. Nonequilibrium

(a) Q_{HS} - thermal inventory of heat source

Q_{LOSS} - heat losses through insulation, gaps, module cladding, supports

T_{RAD} - fin root temperature of radiator

T_C - Cold-junction temperature of thermopile

T_H - hot-junction temperature of thermopile

h - radiator convection and conduction heat transfer coefficient

T_b - boundary temperature

P_e - electrical output power of thermopile

R_{LOAD} - external electrical load

k_{INS} - thermal conductivity of thermal insulation

$\delta P_E/\delta t$ - rate of output power degradation

S,ρ,k,ρ_c - Seebeck coefficient, electrical resistivity, thermal conductivity, and electrical contact resistivity of thermoelements.

A_x - cross-sectional area as a function of position on thermoelement.

duration of solar incident flux (or planetary albedo) may be sufficiently small that the RTG operates under nonequilibrium conditions. In this case, the analysis of the RTG can be effected only by performing transient thermal analysis during the initial period (or, the entire duration) of the incident thermal flux.

Secondly, one of the transient effects, viz, the solar incident flux (or planetary albedo), has an asymmetric effect on the operation of the RTG. For example, a solar flux imposed on one side of the RTG may result in significantly higher operating temperatures. Hence, the performance of the RTG, viz, the output power of the thermopile, may vary with position relative to the region of incident flux. In order to assess the importance of asymmetric effects, an initial analysis of RTG performance was effected by modeling the entire RTG to include circumferential as well as radial and longitudinal heat transfer. Although the generator casing or shell is often thick enough to effectively distribute the localized incident heat flux over the entire shell surface, the radiator fins must dissipate essentially all incident heat flux. The above considerations have become the preliminary basis for the development of the RTG analytical model.

The next step in the model development involved the integration of the various analysis routines needed for the transient analysis. The principal analysis routines included in TRANRTG are (1) GESPGN RTG weight optimization program, (2) OFFOPT thermoelectric performance analysis program, and (3) TRUMP numerical differencing heat-transfer program. The interaction of these analysis routines is shown schematically in Figure 1. Functionally speaking, the OFFOPT computer program will initially compute the thermopile operating characteristics based on the initial operating temperatures, thermoelectric properties, external load, junction resistances, and thermoelement length and cross-sectional area. The results of the initial thermoelectric analysis together with user input design constraints are next transferred to the GESPGN program. The GESPGN program initially designs a partially or fully weight-optimized RTG. At this point, the collective results from OFFOPT and GESPGN are transferred to a model generation program (DATAGEN) which translates these above results into a network thermal model and in a format compatible with the input requirements of the TRUMP heat-transfer program. A sequence of initializing refinements to the thermal model follow (see Figure 1) which affords congruency between the RTG "designed" by OFFOPT and GESPGN, and the thermal model created and analyzed by DATAGEN and TRUMP. After "initialization" has been completed, the user's supplied transient data sets are sequentially processed in OFFOPT (see flow chart shown in Figure 1). In this final phase of the transient analysis, the OFFOPT thermoelectric analysis program is coupled to the TRUMP heat-transfer analysis program in order to initially provide (and adjust with subsequent transients) the "effective"* thermal conductivity of the thermopile

*The "effective" thermal conductivity of thermoelectric elements under conditions of finite current flow differs from the conventional material thermal conductivity since Peltier, Thomson, and Joulean thermal transport terms (or sources) need be considered, as well as heat transfer by conventional thermal-conduction process.

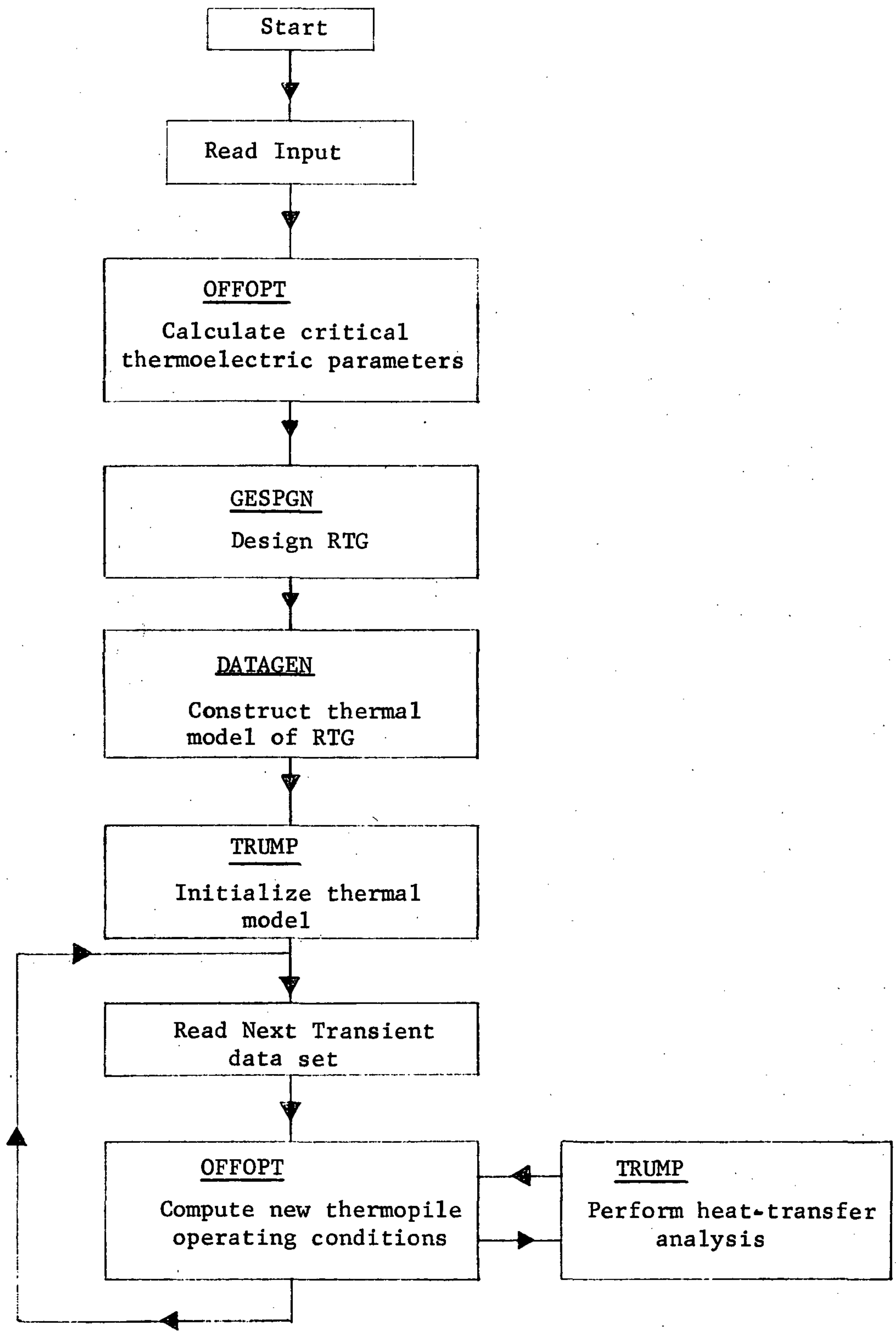

FIGURE 1. TRANSIENT RTG (TRANRTG) MAIN PROGRAM FLOW CHART

OVERLAY	NAME	DESCRIPTION/REFERENCE
0	TRANRTG	Main control program; sequentially calls each of the overlays in order to initialize the problem and finally perform transient analyses. (This program was developed under present study)
1	GESPGN	RTG design optimization program for either (1) detailed weight optimization of RTG or (2) generation of required input data for specified (e.g., previously optimized) RTG. (See Eggers, P. E., "An Advanced Thermoelectric Life Test and Evaluation Study", NASA-GSFC Contract No. NAS 5-10497, Final Report, September, 1968; also "The Analysis and Design of a High-Temperature Thermoelectric Conversion Device", BAT-5-6397-2, Final Report for Contract NAS 5-36971, 1965)
2	DATAGEN	Converts thermoelectric performance parameters/dimensions computed in OFFOPT and RTG dimensions computed in GESPGN to input format compatible with TRUMP heat-transfer computer program. Also, DATAGEN computes radiation view factors for radiator system including shell/fin interactions. (This program was developed under present study)
3	OFFOPT	Performs detailed thermopile thermoelectric analysis using finite-staging energy-balance techniques. (See Best, R. E., "Development of an Analysis Technique for Predicting the Operating Characteristics of Thermoelectric Heat Engines", Thesis, Department of Electrical Engineering, Ohio State University, 1970); "Progress on the Development of Segmented PbTe-Bi$_x$Te Thermoelectric Modules", AEC Contract W-7405-eng-92, BMI Report No. BMI-1794 (January, 1967).
4	TRUMP	Performs heat transfer of the RTG thermal model constructed in DATAGEN. (See Edwards, A. L., "TRUMP Computer Program", Lawrence Radiation Laboratory Report Number UCRL-14754 Revision II, 1969)

FIGURE 1. (Continued)

and the electrical output power, i.e., the amount of thermal energy converted to electrical energy. The effective thermal conductivity of the thermopile is a significant parameter in the thermal analysis since (1) 80 to 90 percent of the thermal inventory is transferred through the thermopile and (2) the effective thermal conductivity of the thermopile can vary substantially with changes in the external load, changes in the thermal and electrical properties of the thermoelectric materials, or changes in the operating temperatures.

The design of the RTG thermal model for purposes of heat-transfer analysis is critical since (1) too coarse a nodal network structure will render the model unresponsive to real transient effects and (2) too fine a nodal network structure will make the computer costs (for a comprehensive RTG transient analysis) prohibitively high. One step taken to reduce the overall number of nodes (hence, computational costs) in the model involved the replacement of a three-dimensional model of the actual system by a two-dimensional model. A review of previous studies* of typical axial temperature profiles of an RTG indicated that the axial temperature gradient in the region of interest, viz, the region including the thermoelectric modules or elements, could be neglected by using average temperatures for the cross-sectional temperature profile. Hence, the present heat-transfer analysis model for the RTG was reduced from a 3-D geometry (see Figure 2) to a 2-D geometry (see Figure 3).

The analysis model shown in Figure 3 includes the major components present in a typical RTG. Although not shown, the nodal network of this model includes the entire cross section of the RTG. This 2π geometry was initially required in order for the analysis to accommodate the asymmetric temperature profile that will be indiced when solar flux or planetary albedo is incident on one side of the RTG.

As discussed above, steps were taken in the design of the RTG heat-transfer model to insure that the nodal network be fine enough, i.e., sufficiently detailed to permit meaningful transient heat-transfer analyses while not requiring prohibitively long (i.e., expensive) computer running times. However, in addition to the above computer-running-time (cost) considerations, it was also necessary to rationally select** the energy-balance criteria that must be specified within the TRUMP heat-transfer computer program. These criteria are critical in that they represent the tradeoff between the "accuracy" of the computed temperature profiles (for the RTG model) and the computer "running time" consumed in the course of the heat-transfer analysis. The computer running time required

---

* Eggers, P. E., "An Advanced Thermoelectric Life Test and Evaluation Study", NASA-Goddard Contract NAS5-10497, September, 1968.

** This process involves using the TRUMP program to perform a series of heat-transfer analyses on typical RTG designs.

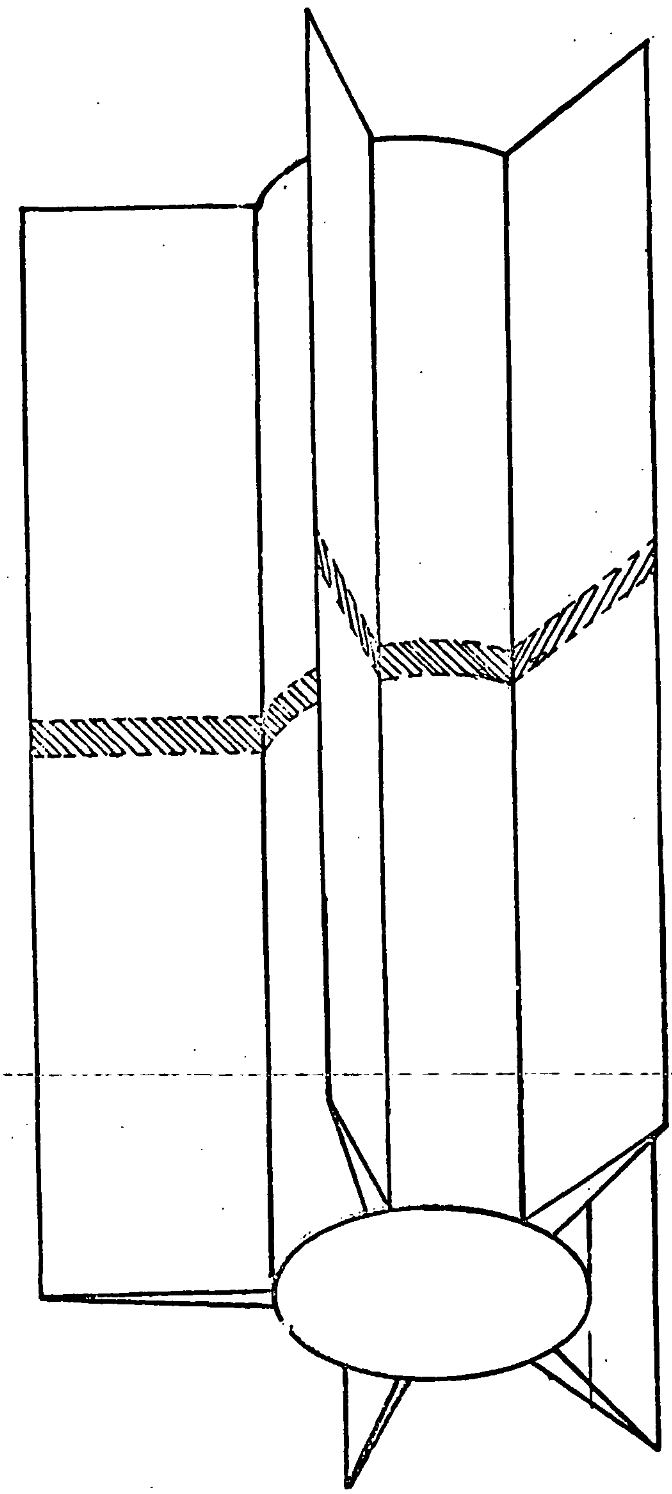

FIGURE 2. LONGITUDINAL VIEW OF RTG SHOWING REGION INCLUDED IN TWO-DIMENSIONAL HEAT-TRANSFER ANALYSIS (Shaded Region)

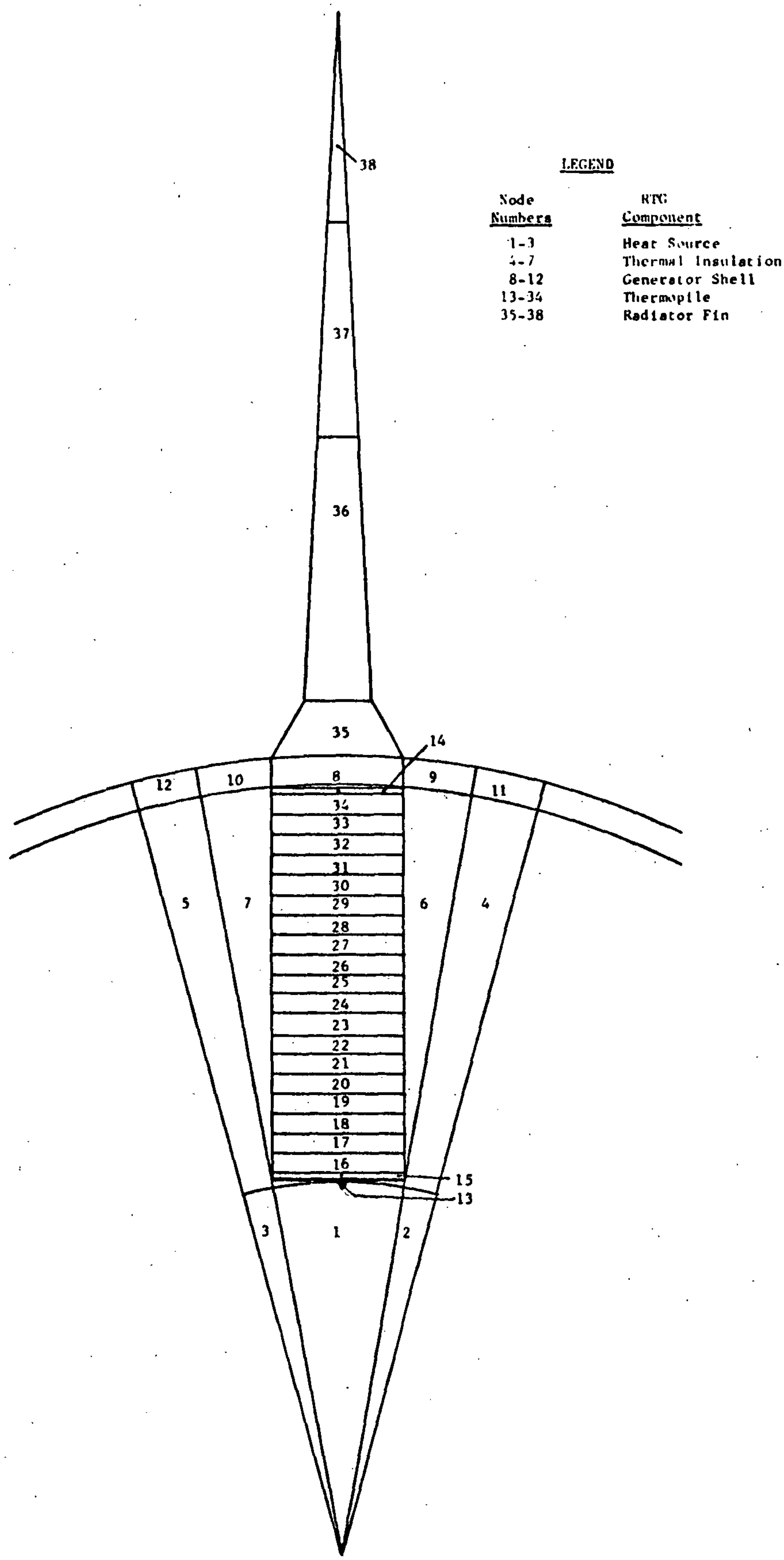

FIGURE 3. 2-D MODEL FOR THERMAL ANALYSIS OF RTG'S

for the heat-transfer analyses is particularly acute in the present case since they will be repeatedly performed at each stage of the transient analysis of a given RTG.

Modeling the Radiator. The thermal modeling of the RTG radiator component* involves the computation of radiation interchange factors or "view factors" for a given number, height of radiator fins and generator shell diameter. These view factors allow the thermal model to accurately represent the radiation interchange between radiator fins. However, the computer makes an adjustment to the effective radiator surface available during the "initialization" phase. This adjustment is necessary since the two-dimensional "slice" out of the RTG (see Figure 2) does not include the heat-dissipation area normally available at the end regions of the RTG. This adjustment in no way interferes with obtaining realistic responses of the radiator component to changes in boundary conditions or surface emittance/reflectance conditions.

A series of 2π geometry heat-transfer analyses was performed in the present study to assess the effects of asymmetric solar flux on the circumferential temperature distribution of typical RTG's. The results of this study indicated that, at distances of one astronomical unit (9.287×10^7 mi) or greater from the sun, and for radiator reflectances of ≥ 0.75, asymmetric effects on the temperature profile of the RTG were on the order of a fraction of a percent and can therefore be neglected. The ability to neglect asymmetric effects is an important simplification in the present computer program since it permits the analyst to construct a thermal model involving a "sector" of the total RTG cross section (see Figure 3) as opposed to the complete 2π geometry of the thermal model. In terms of computer running time, this simplification of the transient RTG analysis will result in a five- to ten-fold reduction in running time.

Modeling the Thermopile. In the process of adapting the OFFOPT thermoelectric analysis subprogram** to the present RTG transient-analysis program, major refinements in the treatment of certain degradation phenomena were made. The first refinement was adding the capability for accommodating sublimation of thermoelectric materials. This capability permits the analyst to study the effects of sublimation (e.g., the loss of thermal and electrical contact area as well as increased electrical resistance in the eroded region) by specifying only the temperature-dependent evaporation rate. The OFFOPT computer program automatically adjusts for induced changes in the temperature distribution along the thermoelectric element as well as the changes in the peripheral surface area available for evaporation. This particular refinement will permit the analyst to evaluate the effect of thermoelement sublimation on RTG performance.

---

* See reference for GESPGN in Figure 1.

** See reference for OFFOPT in Figure 1.

Another refinement to the OFFOPT thermoelectric analysis subprogram introduces the capability to input empirically derived thermoelectric property changes, with time. These changes may include the Seebeck coefficient, electrical resistivity, electrical contact resistivity, and/or thermal conductivity as determined by various diagnostic techniques such as laser-pulse thermal-diffusivity techniques, traversing thermocouple thermal-conductivity measurement techniques, van der Pauw electrical resistivity measurement techniques, and "miniature-specimen" Seebeck coefficient measurement techniques.* In order to make this aspect of the RTG transient analysis more realistic while not placing unreasonable demands on previously measured thermoelectric-property measurements, the normalized** property changes are introduced in four regions of the element. For example, posttest thermoelectric-property measurements may reveal that the p-type leg decreases in Seebeck coefficient and electrical resistivity by 10, 4, 1, and 0 percent in the hot, medium-hot, medium-cold, and cold regions of the element, respectively. By introducing these measured and normalized property changes (probably with an attendant change in thermal conductivity) to the TRANRTG code, the analyst is able to study the effect(s) of thermoelectric degradation on RTG performance with or without the presence of other transient effects.

Changes in the external load of the RTG can be simulated by specifying a normalized change in the external load in the degradation data set. OFFOPT is designed to compute the appropriate thermoelectric-performance parameters based on an external load ranging from open-circuit conditions to short-circuit conditions. The TRUMP heat-transfer program can accommodate this transient operating condition and, by interacting with OFFOPT (which supplies the appropriate effective thermopile thermal conductivity) provides the analyst with time/temperature profiles and time/thermopile performance profiles during the transient period.

Input/Output

The input data for the TRANRTG computer program can be divided into four groups as follows: (1) a set of permanent data containing radiator design parameters for GESPGN; (2) a set of thermoelectric data including thermoelectric property data, initial external load, initial operating temperatures, junction resistances, coefficients and exponents for evaporative erosion, and radioisotope halflife; (3) a set of data to specify the constraints for the RTG design optimization, or simply a specific RTG design if no design optimization is desired; and (4) one or more degradation data sets specifying accumulative elapsed time, normalized changes in thermoelectric properties, emittance changes, multiplying factors for evaporative erosion rates, temperature exponents of contact resistivity, normalized thermal insulation thermal conductivity changes, normalized external load changes, and incident solar flux.

---

* These diagnostic methods have been developed at Battelle's Columbus Laboratories under previous thermoelectric contracts.

** Normalized property changes determined by dividing property value at time t, by property value at time t_0, corresponding to beginning of life of RTG.

The output data from TRANRTG include principally (1) the initial thermopile performance parameters, (2) the results of RTG design optimization, characteristics corresponding to various transient conditions or degraded conditions for the RTG. The results of sample transient analysis calculations that appear in Appendix B illustrate the detailed output data display provided by the TRANRTG computer program. Specifically the transient output data include the (1) elapsed time, (2) thermoelectric couple and overall RTG output power and energy conversion efficiency, (3) normalized RTG output power, (4) specific power, internal resistance, and electrical current of RTG, (5) thermoelectric properties and element cross-sectional dimensions as a function of temperature and axial position, and (6) temperature profile of the RTG sector analyzed (corresponding to the thermal model shown in Figure 3). Hence, the present computer program provides a prediction of the RTG operating characteristics and thermopile condition (thermophysical properties and dimensions) at selected intervals of time.

Sample Transient Analyses

The results of a sample set of transient analyses of a 250-watt(e) RTG involving radioisotope decay and sublimation of the thermoelements are in Appendix A. The RTG selected for these analyses is characterized by (1) 2p - and 2n - PbTe thermoelements, (2) nominal cold- and hot-junction temperatures of 500 and 800 K, respectively, and (3) sublimation rates over the range 0 to 3 percent of the free-sublimation rate for PbTe. The results of sample calculations such as shown in Figure 5 could be compared with observed RTG operative characteristics in order to verify or refute a given set of hypothesized degradation mechanism(s). Once the degradation mechanism(s) have been confirmed, the hypothesis may be applied to RTG designs of differing configurations in order to predict expected RTG performance under anticipated transient conditions (as summarized in Table 1).

No comparison of the predicted RTG performance with observed RTG performance profiles can be made at the present writing since a meaningful comparison requires a thorough knowledge of all of the mechanisms contributing to the overall change in RTG performance. Specifically, a thorough comparative analysis would require (1) RTG operating characteristics (open-circuit voltage, internal resistance, output power, and possibly thermopile temperatures) as a function of time and (2) posttest measurements of element cross-sectional dimensions as a function of axial position, (3) posttest measurements of thermal-insulation thermal conductivity, and (4) assessment of changes in thermoelectric properties and junction resistances (based on posttest measurements). It is noteworthy, however, that the principal analysis subroutines used inthe TRANRTG computer program, i.e., the OFFOPT thermoelectric analysis subroutine and the TRUMP thermal-analysis subroutine, have been qualified by independent comparative analysis studies.**

---

* Bates, H. E. and Weinstein, M., "Evaporation Rates of PbTe and PbSnTe Pressed and Sintered Thermoelements", Proceedings of IEEE/AIAA Thermoelectric Specialists Conference, Washington, D.C. (May, 1966).

** See references (10) and (11) on page 34.

Task II. Fabrication and Performance Testing of SiGe-PbTe Segmented Thermoelectric Generators

Introduction

Theoretical analyses have shown that SiGe and PbTe thermoelectric materials, when used in segmented-element form, offer a significantly higher energy-conversion efficiency than is obtainable with either material used separately. Such analyses, however, presuppose the existence of a segmented-couple configuration with low contact resistance. A thorough evaluation of the requirements for segmenting SiGe and PbTe has revealed the following associated problems: (1) SiGe and PbTe differ in thermal expansivity by a factor of four which, therefore, complicates the direct bonding of each material to a common intermediate transition member, (2) the processing temperatures associated with the bonding of metal shoes to SiGe and PbTe are not in general, compatible, and (3) the selection of candidate shoe materials for PbTe, particularly p-type PbTe, is limited by its tendency to be poisoned by most metals.

Previous efforts to effect low-contact-resistance bonds at the SiGe/PbTe interface have met with only limited success, with mechanical failure frequently occurring in handling or the thermal cycling experienced during subsequent evaluative testing. However, a totally new concept in the design of segmented couples has been developed which incorporates pressure-contacted junctions at the SiGe/PbTe and SiGe/hot-strap interfaces. Thus, the complicated transition members, which are otherwise required to join materials of greatly differing thermal expansivities, have been eliminated. In the present concept, the W/SiGe bonded composite is pressure contacted to PbTe and exhibits and electrical contact resistivity of only 100 to 200 μohm-cm^2 at 800 K--which is equivalent to a loss of 20 to 40 milliwatts of output power for thermoelectric couples operating at a current flux of $\sim$ 10 amps/cm^2.

In the present study, hermetically sealing bellows enclosures, i.e., "modules", have been introduced to implement the SiGe-PbTe segmented-couple concept involving pressure-contacted junctions. The bellows enclosures provide (1) the spring-loading pressure required to effect low-resistance, pressure-contacted junctions, (2) a means for isolating the individual thermoelectric elements from the potential sources of contamination within the thermoelectric generator, and (3) a means for operating the thermoelectric elements at inert-gas overpressures of 75 to 150 psia.

The advantages of operating thermoelectric elements at an overpressure of an inert gas have already been demonstrated by research conducted by Sandia Laboratories.* Specifically, it has been shown that the rate of evaporative erosion of thermoelectric materials is approximately inversely proportional to the inert-gas pressure. For example, by increasing the internal pressure of the thermoelectric-element environment from 15 psia to 60 psia, the evaporation rate would decrease by 75 percent.

---

* References are listed on page 34

Present generator designs limit the internal pressure to usually 30 psia or less. However, as mentioned above, the miniature bellows which encapsulate the thermoelectric elements are designed to withstand internal pressures of up to 150 psia while maintaining the desired amount of spring-loading pressure.

An additional advantage of the hermetically sealed bellows module concept is that of minimizing the possibility of gaseous contamination, e.g., from oxygen-contaminated thermal insulation materials. Studies performed by the author[2] have revealed that the preferential Te sublimation rate in p-type PbTe thermoelectric materials is as much as several orders of magnitude higher in an oxygen-containing argon atmosphere than in a pure inert or reducing atmosphere. Based on our findings[2], this preferential sublimation of Te from the p-type PbTe has been found to be the principal contribution to degradation during thermoelectric life tests. On the other hand, the operation of PbTe thermoelectric couples at a hot-junction temperature of 750 K in a reducing hydrogen atmosphere permitted stable operation (<10 percent degradation in output power) for periods in excess of 18,000 hr. According to the author's hypothesized degradation model[2], the hermetically sealed module concept will afford a comparable or better level of performance stability.

The availability of materials suitable for use in fabricating the bellows is one of the most critical factors in demonstrating the reasibility of this enclosure concept. Studies performed under NASA Contract NAS3-0421[3] have indicated that Inconel 718 shows adequately low relaxation and good performance in vacuum at temperatures of 1000 F for periods exceeding 2000 hr. Hence, the key component in this concept, viz, the bellows, was fabricated using Inconel 718. The convoluted section of the bellows was used only up to 1000 F; straight tubing was used between that point and the hot platen (see Figure 4). The increased heat-path length afforded by the bellows convolutions together with the low thermal conductivity of Inconel 718 ($\sim$ 0.20 watts/cm C at 500 C) results in moderate bypass heat losses ($\sim$ 10 to 15 percent). The remaining components are presently accepted materials for use in a thermoelectric SiGe-PbTe segmented couple draw on previously developed technology. The principal exception is the SiGe/hot-strap design which was designed with a graphite hot shoe; the use of $MoSi_2$ hot-strap technology associated with RCA air-vac thermocouple technology would be expected to result in improved hot-junction performance.

In the following discussion, attention is focussed on the design, fabrication, and evaluation of the SiGe-PbTe segmented couples involving hermetically sealing bellows enclosures.

Design of Segmented Couple

The design of the SiGe-PbTe segmented couple presented below has evolved based on technology developed over the course of several NASA-Goddard

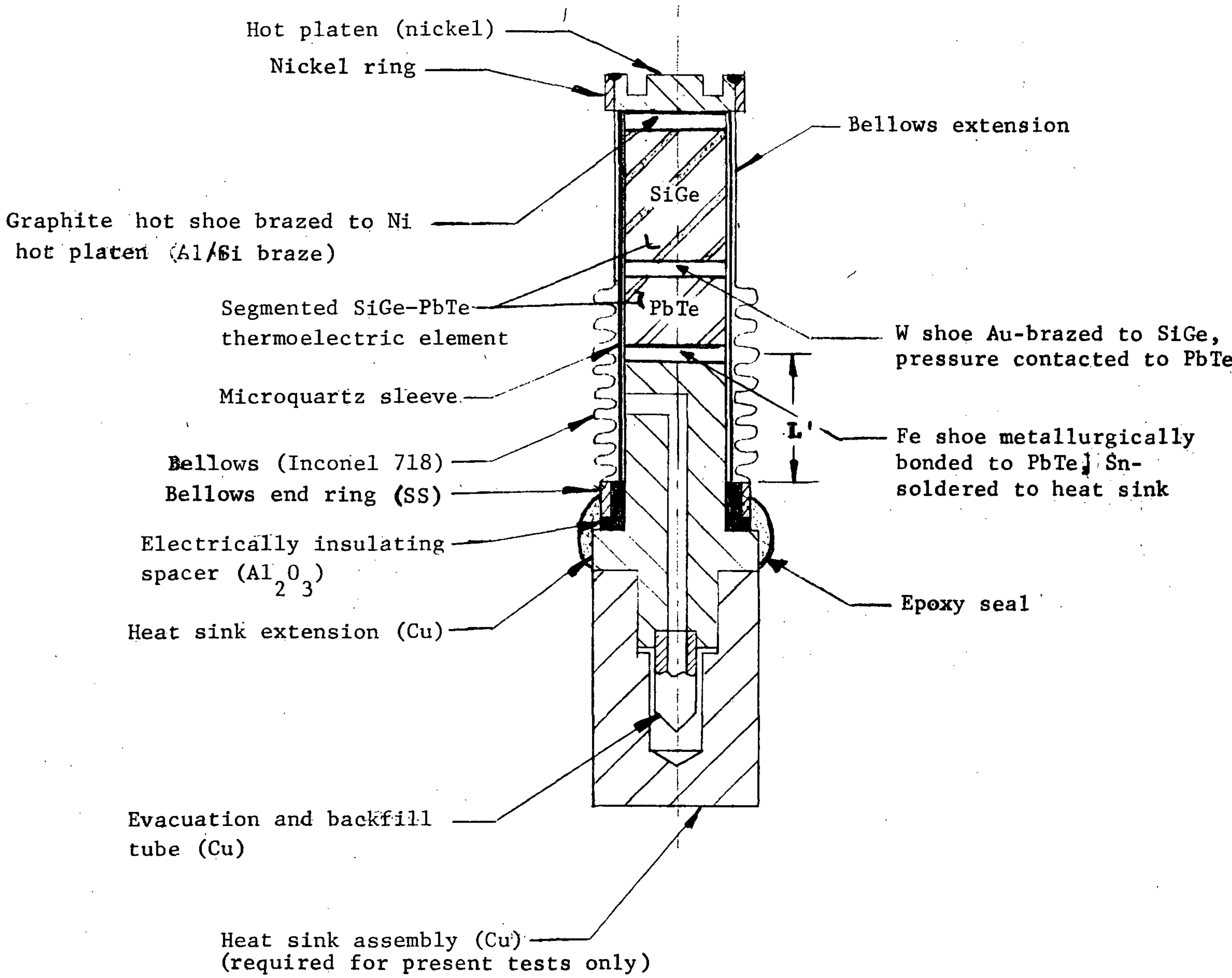

FIGURE 4. BELLOWS-ENCAPSULATED THERMOELECTRIC ELEMENT FOR USE IN LIFE-TEST EFFICIENCY MEASUREMENT APPARATUS

sponsored research programs[(4-7)]. One encapsulated element of this segmented couple design[(5)] (see Figure 4) features pressure-contacted junctions (1) between the PbTe segments and the tungsten shoe (which is bonded to the cold end of the SiGe segments) and (2) between the SiGe segments and the high-purity graphite hot strap. The use of a pressure-contacted junction eliminates the problem of mismatched thermal expansivities encountered in previous SiGe-PbTe segmented-couple development. In addition, this design simplifies the couple-fabrication schedule since the SiGe and PbTe segments can be processed separately and assembled upon installation of the couple(s) into either a generator or test fixture. In addition, an axial, compressive-loading pressure 125 to 150 psi is required during the operation of the segmented couple and is effected through the use of specially designed bellows enclosures. This level of axial loading pressure is necessary to effect low resistance at the pressure-contacted junctions.

Specifically, a theoretical analysis was performed using the OFFOPT computer program in order to identify the dimensions of the SiGe and PbTe segments yielding maximum energy-conversion efficiency for a given overall element length. The input data used for the PbTe (2p- and 2n-PbTe) segments were based on Seebeck coefficient, electrical resistivity, thermal conductivity, and electrical contact resistivity measured at Battelle's Columbus Laboratories. The input data for the SiGe (containing 80 percent Si) segments was based on RCA-published data. The results of the calculations are summarized in Table 2 in terms of operating temperatures, couple dimensions, output power, and conversion efficiency. These elements were sized for insertion into the bellows assemblies described in detail below.

Design of Bellows Enclosure

The next step in the development of a bellows-encapsulated segmented couple involved the optimization of the design of the bellows enclosure. ~~First, a literature search was conducted in order to identify candidate~~ materials for use in construction of the bellows. It was found that, in studies performed under NASA Contract NAS3-9421[(8)] involving 6-8 metals and alloys, Inconel 718 exhibited the lowest relaxation when operated in vacuum at temperatures of 1000 F for periods in excess of 2000 hr. Based on these results, and its other desired mechanical properties, Inconel 718 was selected for use in the fabrication of the bellows enclosures.

Having identified the material to be used in fabrication of the bellows, the next step involved optimizing the wall thickness of the bellows. The principal considerations in optimizing the wall thickness included (1) the by-pass heat losses should be minimized, hence, the wall thickness should be minimized, (2) the spring-loading capability of the bellows requires certain minimum wall thickness, and (3) the resistance to creep and creep rupture should be maximized, hence the wall thickness should be maximized (to minimize applied force per unit area).

A heat-transfer analysis was performed based on the model shown

TABLE 2. COMPUTED DIMENSIONS AND PERFORMANCE PARAMETERS FOR SiGe-PbTe SEGMENTED COUPLES

T_C	=	450 K
T_{INT}	=	800 K
T_H	=	1175 K
A_P	=	0.535 cm^2
A_N	=	0.535 cm^2
L_N (SiGe)	=	1.25 cm
L_N (PbTe)	=	0.45 cm
L_P (SiGe)	=	1.30 cm
L_P (PbTe)	=	0.40 cm
Thickness (hot strap)	=	0.234 cm
I	=	7.0 amps
P	=	1.30 watts
$\eta_{T/E}$	=	7.97 percent*

* Accounts for heat losses through bellows.

Note:

T	=	temperatures
A	=	cross sectional areas
L	=	lengths
I	=	operating current
P	=	output power (electrical)
$\eta_{T/E}$	=	conversion efficiency
N,P	=	n-type and p-type thermoelements
C,INT,H	=	cold-, intermediate-, and hot-junction temperatures, respectively

in Figure 4* for SiGe-PbTe segmented elements. The purpose of this analysis was to estimate the "bypass" heat losses through the bellows wall for various bellows wall thicknesses, thermoelectric element lengths, and heat-sink extension lengths. It is noteworthy that the heat-sink extension length, ℓ', is that length which extends above the base of the bellows and is adjacent to the bellows (see Figure 4). The purpose of the heat-sink extension is to increase the effective heat-transfer-path length through the bellows. The results of these heat-transfer analyses are summarized in Figure 5 and illustrate the expected influence of bellows wall thickness and heat-sink extension length, ℓ'. The influence of thermoelectric element length on the heat loss through the bellows is the combined result of (1) the decreasing thermal flux through the thermoelectric element with increasing length, hence, the bypass losses become a greater fraction of the total heat transferred and (2) the increasing heat-transfer path length with increasing element length. As can be seen from Figure 5 the heat-transfer path-length effect is dominated by the thermal flux effect. The net result is an increasing fractional heat loss through the bellows with increasing element length.

The selection of a typical thermoelectric element length of 1.7 cm, a heat-sink extension length** of 1.2 cm, and a bellows wall thickness*** of 0.0109 cm (~ 4.4 mil) yields a bypass heat loss through the bellows of ~10 percent. This calculated heat loss is not as substantial as would appear at first glance. First, the bellows may permit the thermoelectric material to be operated at a temperature substantially higher (in terms of increased energy-conversion efficiency) than attainable otherwise. For example, consider the Transit RTG concept, which, due to its designed operation in vacuum, is limited to hot-junction temperatures of ~ 400 C. Second, the generator may now be able to utilize vacuum foil "super" insulations in the spaces between the bellows-encapsulated thermoelectric elements in place of higher-thermal-conductivity (and often contaminated) fibrous, thermal insulations. Third, the bellows-encapsulated thermoelectric elements may be used to attach "unitized" heat sources with "shaped" hot shoes which cover a higher percentage of the heat-source volume and thus further reduce the heat-loss paths encountered in a conventional generator design. The latter concept discussed in more detail below. Finally, the inherently high thermal conductance of this heat-sink design (no sliding contact as required for conventional spring-loaded generators) allows the thermoelectric elements to operate typically 25 to 50 C lower in cold-junction temperature than in conventional spring-loaded generators, and, hence, affords higher energy-conversion efficiency.

* Note that the convolutions (required for spring loading) in this design only extend up to 1000 F temperature and that a cylindrical container is used in the higher-temperature regimes.

** This length includes 0.13-cm-thick cold shoe and intermediate shoe, and a 0.234-cm-thick hot shoe.

*** This thickness is commercially available and is adequate to achieve the desired spring-loading pressure (150 psi) and internal "over pressures" of inert gas.

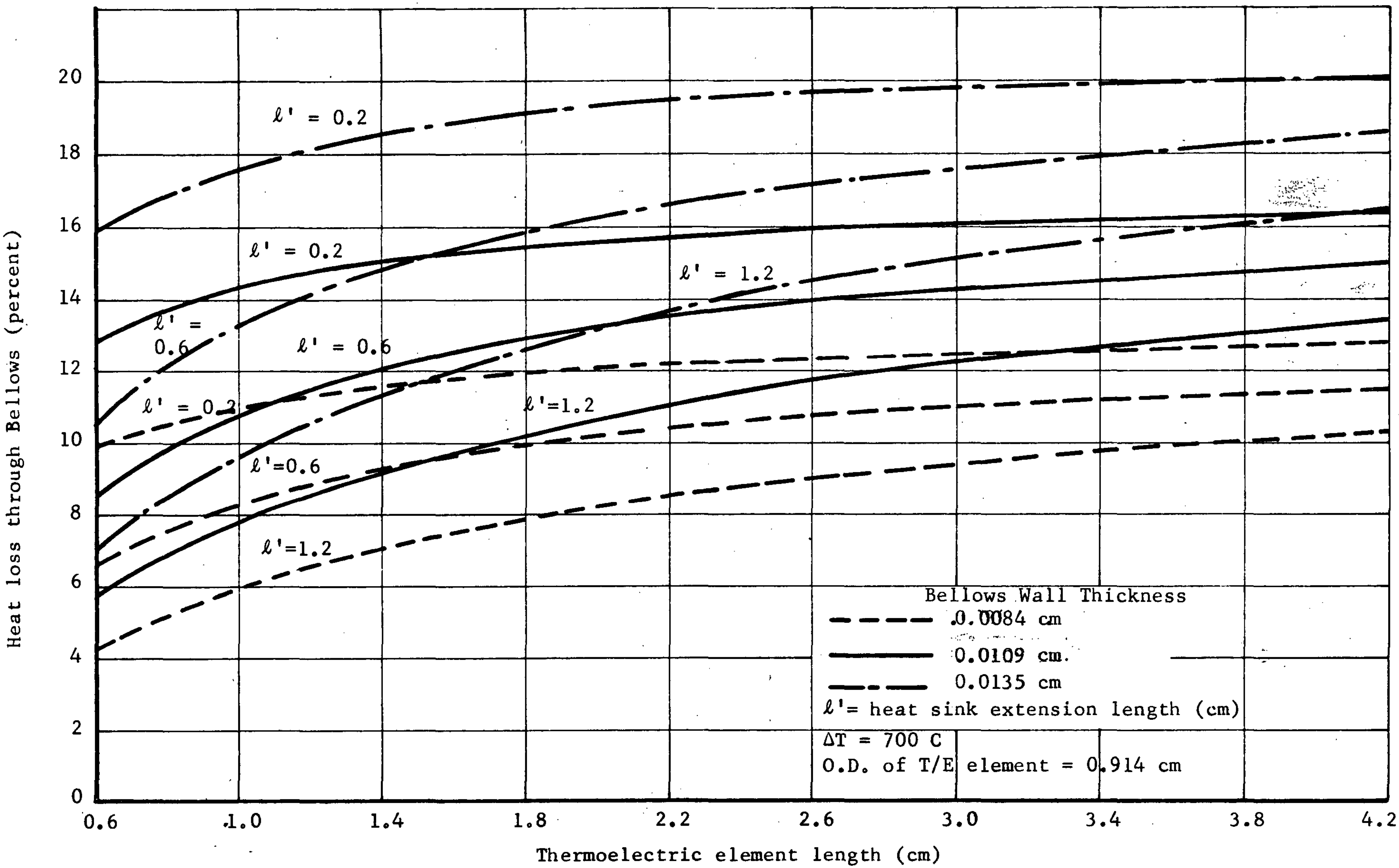

FIGURE 5. HEAT LOSS AS A FUNCTION OF SEGMENTED SiGe-PbTe THERMOELECTRIC ELEMENT LENGTH FOR SEVERAL BELLOWS WALL THICKNESSES AND HEAT-SINK-EXTENSION LENGTHS

The above dimensions, viz, an element length of 1.7 cm, a total heat-sink extension length of 1.2 cm, and a bellows wall thickness of 0.0109 cm were selected for the "proof-of-concept" experimental studies described below.

Fabrication of Bellows-Encapsulated Segmented Elements

A total of four bellows-encapsulated segmented couples were fabricated for performance testing. The bellows enclosures (see Figure 4) were fabricated by TIG-welding nickel hot platens to the as-fabricated bellows subassemblies.*

The thermoelectric elements were fabricated using (1) the 80 percent Si alloy of SiGe and (2) 2p- and 2n-PbTe. The SiGe segments were machined and ground from SiGe ingots purchased from RCA. The PbTe segments were fabricated from PbTe powder purchased from 3M Co. The iron cold shoes were joined to the PbTe segments using powder-metallurgical methods. The SiGe thermoelectric legs and tungsten intermediate shoes were bonded into a composite through the use of gold as a brazing agent. The brazing was accomplished using technology developed in earlier SiGe-PbTe segmenting studies. Specifically, the gold was incorporated in the junctions in the form of a foil. The assembled components were maintained in close contact in a differential-thermal-expansion bonding fixture and were brazed in vacuum for 1/2 hr at 1066 C (1950 F).

Several techniques for joining the graphite hot shoe to the SiGe were studied. High-temperature, high-vacuum ($\sim 10^{-6}$ Torr) bonding trials involving only graphite and SiGe were unsuccessful. The introduction of a thin film of Ge between the graphite and the SiGe did provide a degree of bonding between the SiGe and graphite. The graphite was subsequently brazed to the nickel hot platen using an aluminum-silicon brazing alloy. A composite view of the thermoelectric segments is shown in Figure 6. The components shown in Figure 6 include (from left to right) (1) the PbTe segment with bonded Fe shoe at the cold junction, (2) the tungsten intermediate junction shoe (prior to braze bonding to the SiGe), (3) the SiGe segment, and (4) the graphite disc hot shoe. The thermoelectric elements were next enclosed in a mica sleeve and positioned on the copper heat-sink extension (see Figure 4). This subassembly was next inserted in the bellows enclosure. A specially designed holding fixture allowed the bellows enclosure to be "stretched" the desired amount during which time a high-temperature epoxy seal was effected (see Figures 4 and 7). In this "proof-of-concept" study, an epoxy seal was employed in lieu of the glass/metal seal, e.g., Covar/glass seal, ultimately required for this module concept.

* Supplied by Standard-Thomson Corporation.

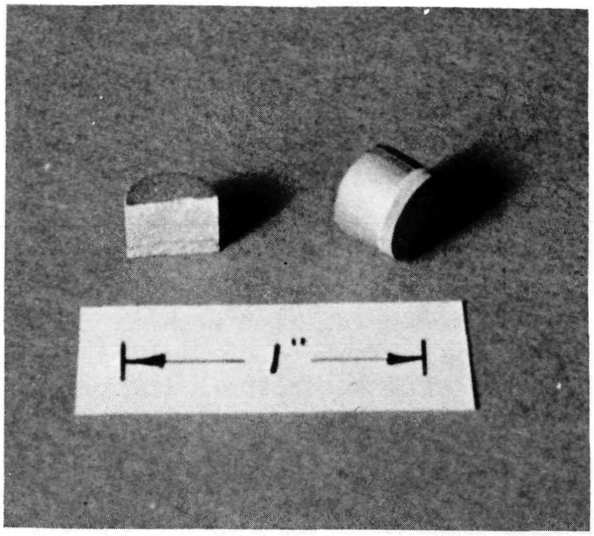

p-TYPE PbTe SEGMENT SHOWING Fe SHOE
AND SnTe LAYER

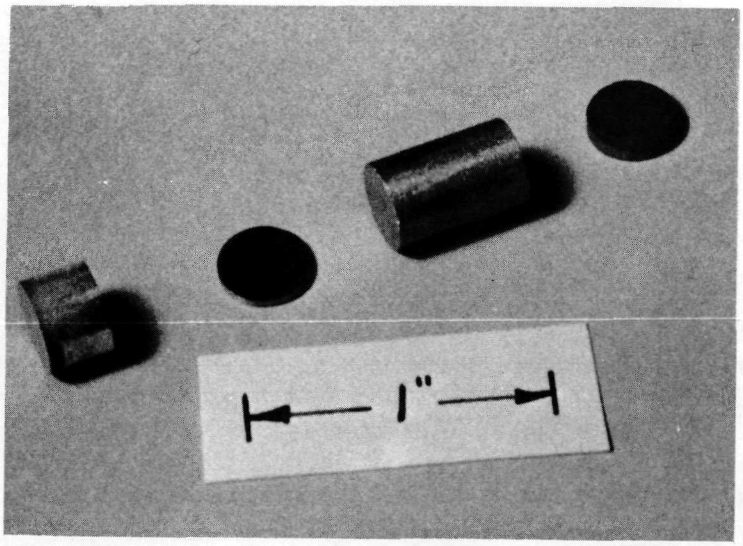

FIGURE 6. VIEW OF SEGMENTED SiGe-PbTe ELEMENT INCLUDING PbTe SEGMENT, W INTERMEDIATE SHOE, SiGe SEGMENT AND GRAPHITE HOT SHOE

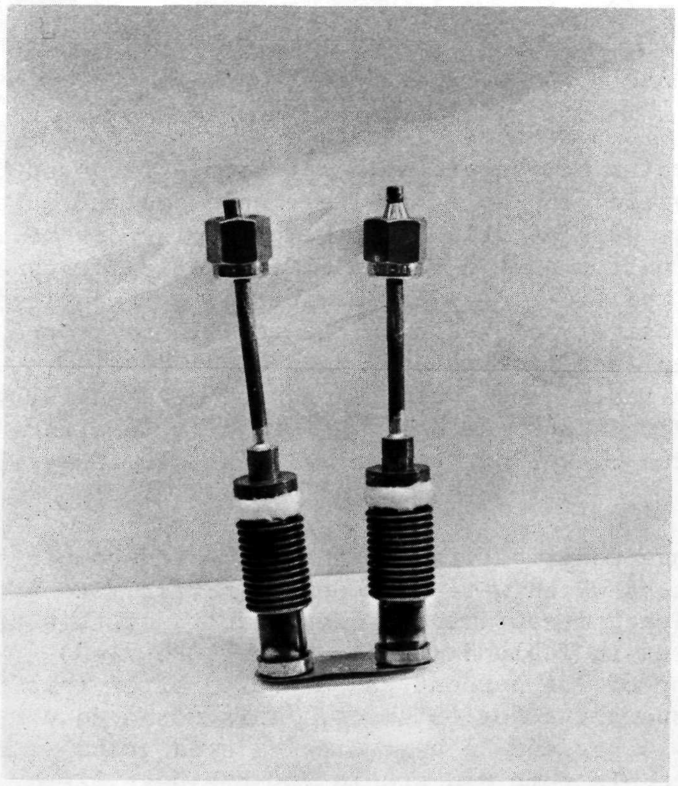

FIGURE 7. BELLOWS-ENCAPSULATED SiGe-PbTe SEGMENTED ELEMENTS SHOWING Ni HOT STRAP AND EVACUATION/FILL TUBES

The bellows-encapsulated SiGe-PbTe segmented elements were next evacuated down to 10^{-6} Torr (at $\sim$ 150 C) and backfilled with research-grade argon (99.9995 percent argon). Following the evacuation and backfill with argon, the bellows-encapsulated elements were sealed by pinching off the evacuation/fill tubes (see Figure 8). The couple was next instrumented with thermocouples and attached to the heat-sink hardware of the life-test efficiency-measurement apparatus shown in the sequence of photographs (Figures 9 to 11) and the shcematic drawing in Figure 12.

Experimental Results

The results of the preliminary "proof-of-concept" experimental studies are summarized in Table 3. The couple designs selected for these evaluation staudes were described in the preceding discussions. The experimental evaluation of two of the SiGe-PbTe segmented couples (Couple Numbers BPG-71-1 and BPG-71-2) was terminated at an early stage of the tests due to excessively high electrical resistance at the hot-shoe/SiGe and hot-shoe/hot-platen interfaces. Subsequent bonding studies revealed that the junction resistance could be reduced substantially by (1) introducing a Ge "bonding agent" at the SiGe/graphite interface and (2) brazing the graphite to the nickel hot platen using an aluminum-silicon brazing alloy.

The above modifications to the segmented-couple design provided junction resistances which were low enough initially to permit meaningful conversion-efficiency measurements. The results of this efficiency measurement are summarized in Table 3 (Couple Number BPG-71-3). An energy-conversion efficiency of 7.6 percent was measured after this SiGe-PbTe segmented couple had been operating for 65 hours. This measured conversion efficiency was approximately 6 percent below the calculated value (i.e., η_{calc} = 7.97 percent). This couple remained stable for the next 120 hr, after which time the output power and conversion efficiency began to decrease. The results of these preliminary tests indicate that additional hot-shoe development will have to be undertaken before long-term tests can be considered. Post-test visual examination of the segmented couple (BPG-71-3) revealed that the difference between the calculated and measured conversion efficiency is probably the result of high junction resistances at the SiGe/graphite interface and/or the graphite/nickel hot-platen interface. As previously indicated, it is expected that use of available MoSi hot-shoe technology would permit long-term operation with low resistance at the SiGe hot junction.

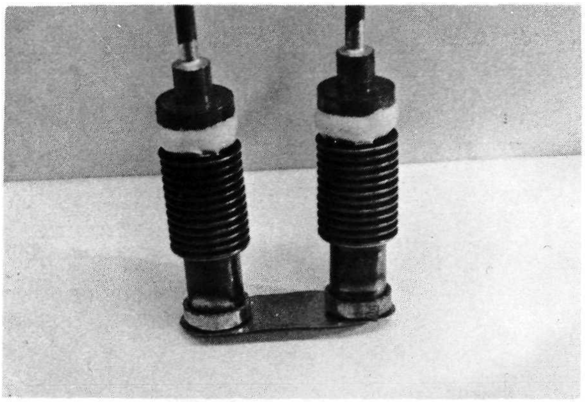

FIGURE 8. BELLOWS-ENCAPSULATED SiGe-PbTe SEGMENTED ELEMENTS FOLLOWING EVACUATION, BACKFILL WITH ARGON, AND CLOSURE

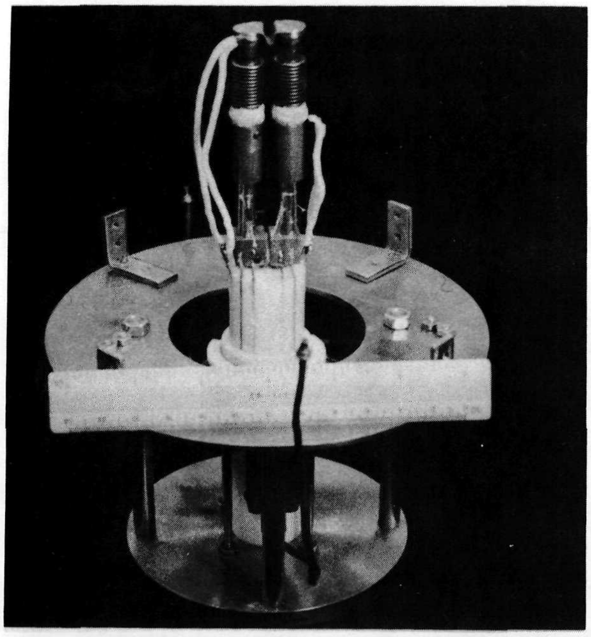

FIGURE 9. LIFE-TEST AND EFFICIENCY-MEASUREMENT APPARATUS WITH SiGe-PbTe SEGMENTED ELEMENTS ATTACHED TO HEAT-FLUX TRANSDUCER/HEAT-SINK ASSEMBLY

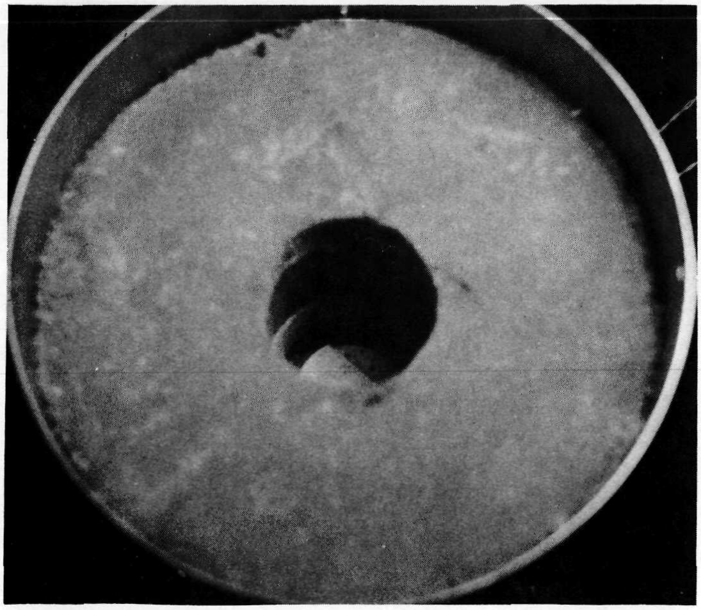

FIGURE 10. LIFE-TEST AND EFFICIENCY-MEASUREMENT APPARATUS SHOWING THERMAL INSULATION AND HEAT-SOURCE/SPECIMEN/HEAT-SINK CAVITY

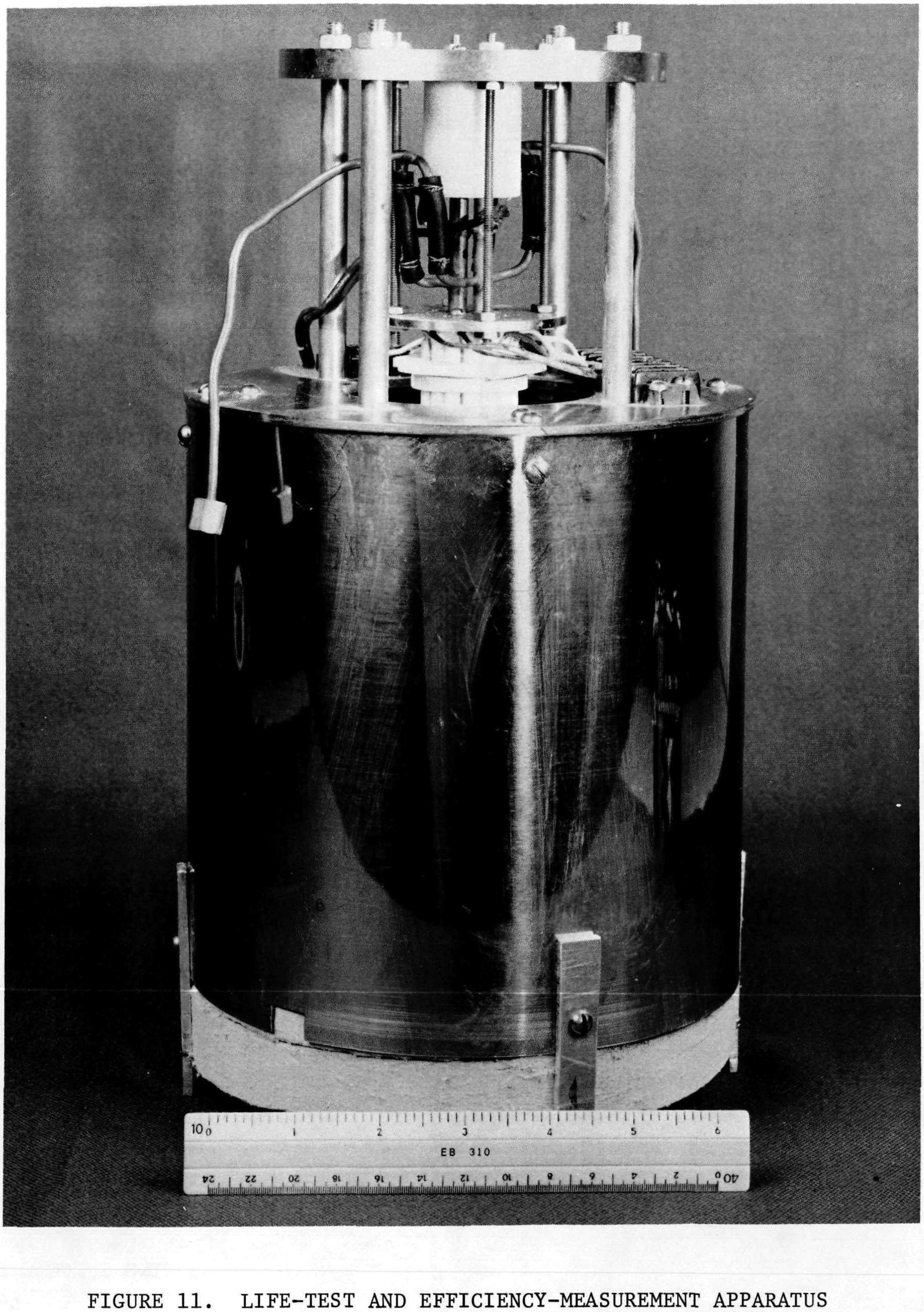

FIGURE 11. LIFE-TEST AND EFFICIENCY-MEASUREMENT APPARATUS WITH SPECIMEN IN PLACE (SPECIMEN INSIDE THERMAL INSULATION CAVITY IS NOT VISIBLE IN THIS PHOTOGRAPH)

1. Heat sink
2. Heat-flux transducers
3. Heat-sink supports
4. Bellows-encapsulated thermo-electric specimen
5. Heat source (Pt wound on Al_2O_3)
6. ZrO_2 powder
7. Min-K 2000
8. ZrO_2 support
9. Cold-junction thermocouples
0. Hot-junction thermocouple

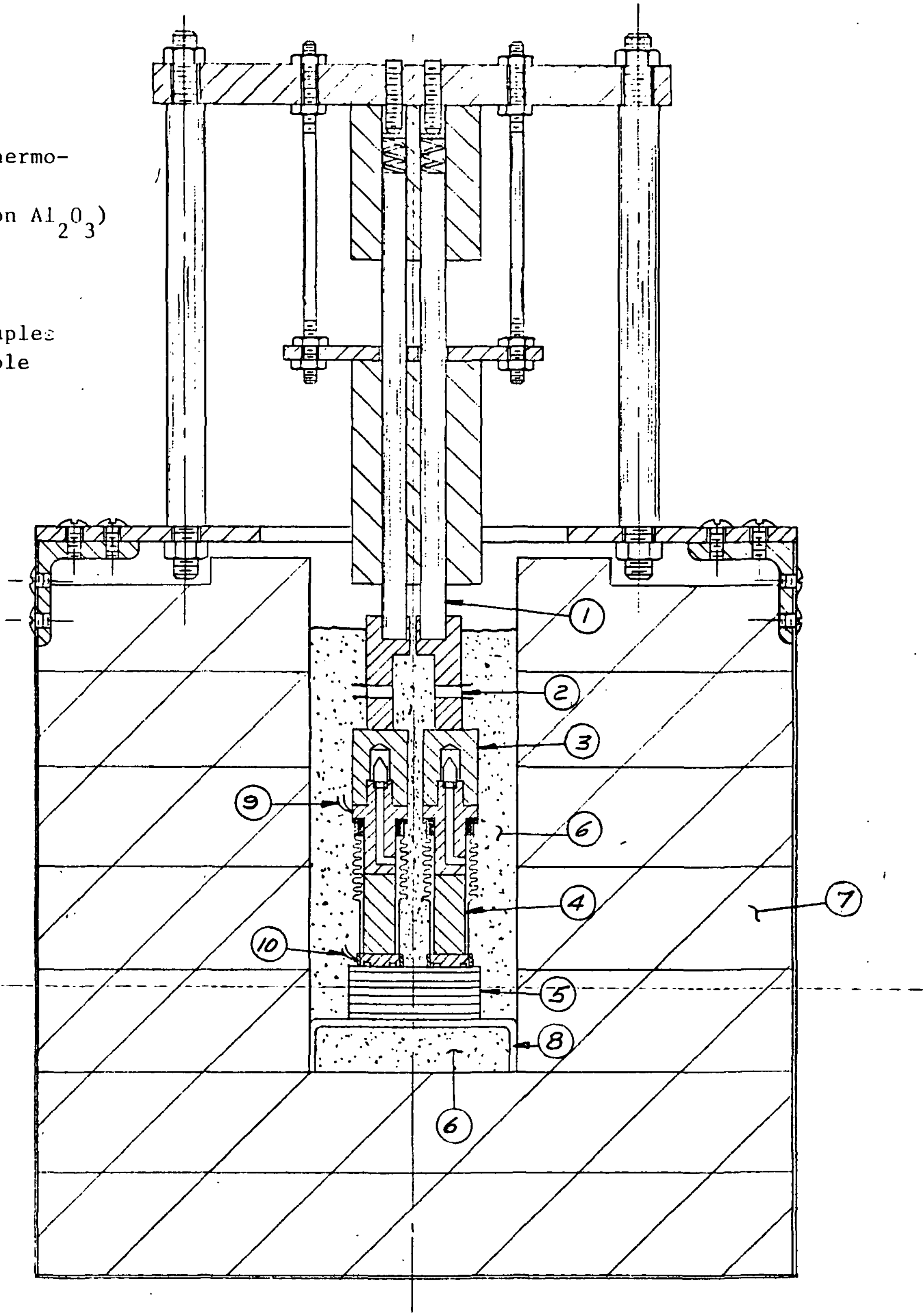

FIGURE 12. LIFE-TEST EFFICIENCY-MEASUREMENT APPARATUS
(All tests performed under vacuum conditions)

TABLE 3. COMPUTED AND MEASURED PERFORMANCE PARAMETERS FOR BELLOWS-ENCAPSULATED SiGe-PbTe SEGMENTED COUPLES

Parameter	Calculated	Measured Results for BPG-71-3
Cold-junction temperature	450 K	441 K
Intermediate-junction temp.	800 K	(not measured)
Hot-junction temperature	1175 K	1208 K
Total heat flow*	16.3 watts (th)	14.5 ± 1.0 watts (th)
Couple output power	1.3 watts (e)	1.1 watts (e)
Operating current	7.0 amps	5.6 amps
Couple conversion efficiency	7.97 percent	7.6 ± .5 percent**

*includes by-pass heat losses in bellows

**As compared with measured SiGe couple efficiencies of 6 - 6.5 percent operating at same cold- and hot-junction temperatures (see "Thermoelectric Materials and Module Development Program", 6th Quarterly Report, ALD(2510)-6 (1969)).

Note: The bellows-encapsulated module concept adds approximately 2 to 2.4 grams to the total weight of each element in RTG. However, this module concept eliminates the need and the weight for the hot frame and the spring-load follower at the cold frame. Hence, the bellows concept should permit a higher specific power. (See Eggers, P. E., "A Unitized Thermoelectric Module Concept", ASME Technical Paper No. 71-WA/Ener-1, (December, 1971))

Task III. Study of Sublimation Barriers for Vacuum Operation of Thermoelectric Elements

Introduction

The evaporative erosion of the thermoelectric materials, particularly the lead-tellurium family of materials, has long been regarded as one of the principal causes of degradation. The high vapor pressure of PbTe has limited its use in vacuum to temperatures of $\sim$ 675 K. In the past, efforts to minimize or eliminate the evaporative erosion of thermoelectric materials have included the use of mica sleeves, quartz "washers", the zero-void, Westinghouse tubular generator concept, and the hermetically sealed SNAP-27 concept.

In the present study, several types of mechancial-barrier schemes are evaluated as a means for suppressing the sublimation of thermoelectric materials in vacuum. The mica-sleeve scheme included in this study is a "reference" condition along with a reference bare element (no mechanical barrier). The effectiveness of the candidate sublimation-barrier techniques is experimentally evaluated by (1) weight-loss measurements, (2) observation of dimensional changes of thermoelectric elements, and (3) posttest Seebeck coefficient traverse measurements. A description of the experimental procedures and the results are presented below.

Development of Sublimation-Barrier Schemes

A total of four sublimation-barrier schemes were included in this experimental study. All of the sublimation-barrier studies involved in-gradient operation of p-type PbTe (sodium doped, with excess tellurium over solid solubility) in vacuum at nominal operating hot- and cold-junction temperatures of 800 K (980 F) and 320 K (113 F), respectively. The p-type PbTe was selected for this present study because of its relatively high vapor pressure and relatively high figure of merit. The thermoelectric elements were fabricated by pressing and sintering p-type PbTe powder (see Figure 13). The "as fabricated" thermoelectric elements were next enclosed in the selected barrier scheme and placed on test.

A study of candidate barrier schemes revealed that the following schemes might afford a significant decrease in the sublimation rate of p-type PbTe: (1) a close-fitting mica sleeve, (2) a close-fitting mica sleeve with Al_2O_3 cement at the mica/W hot-shoe interface, and (3) an oxide-fiber shroud wrapped on a mica-sleeve-enclosed thermoelectric element. A bare element (without any type of sublimation barrier) was also included in this study to provide a reference condition for the thermoelectric element. A detailed description of each of the above three barrier schemes is presented below. All of the barrier schemes involve 0.76-cm-diameter x 1.5-cm-long 2p PbTe specimens with iron cold shoes and tungsten hot shoes (see Figure 13).

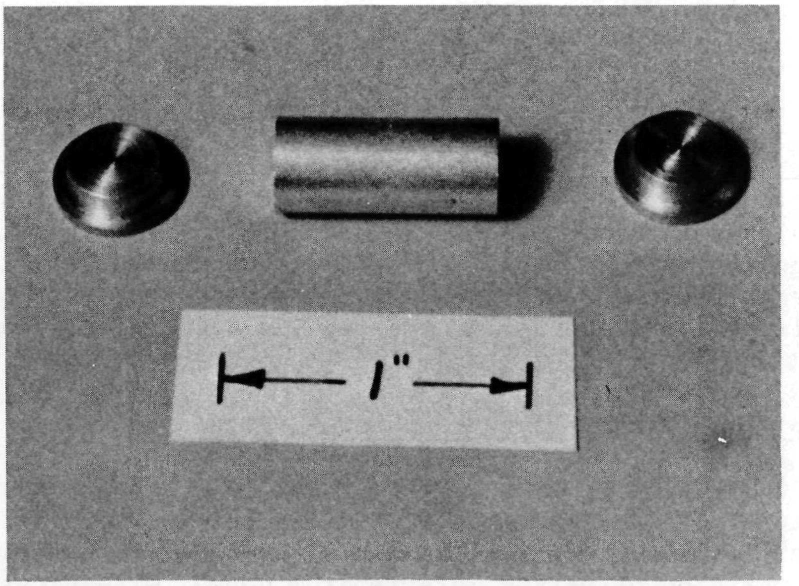

FIGURE 13. BASIC SPECIMEN CONFIGURATION FOR SUBLIMATION-BARRIER STUDIES

Reference Specimens

Two reference specimen configurations have been included in this study, viz, a bare element (no sublimation barrier) and the conventional close-fitting mica sleeve (see Figure 14). The "mica sleeve" barrier scheme involved a close-fitting mica sleeve (10 mil thick) press fit over tapered shoes at either end of the element.

Mica Sleeve with Al_2O_3 Barrier

This barrier scheme is similar to the mica-sleeve configuration described above. However, an additional barrier to sublimation was provided by applying a band of alumina cement at the mica-sleeve/tungsten hot-shoe interface (see Figure 14).

Oxide-Fiber Shroud Over Mica Sleeve

This barrier scheme involved the use of an oxide-fiber shroud over a mica sleeve in order to suppress sublimation of the p-type PbTe specimen. The application of the shroud was accomplished in a two-step process. First, the 2p-PbTe element was enclosed in a close-fitting mica sleeve (10 mil thick) press fit over tapered shoes at either end of the element. Second, the enclosed element was manually wrapped with a shroud of 6 to 7 layers of SiO_2 fibers (containing approximately 18 filaments of nominal 5-μm diameter) (see Figure 14). This approach offers the advantages of minimizing the gap at the openings between the barrier and specimen and provides a "tortuous path" for the transport of the thermoelectric material from the surface of the specimen. For example, in the case of the mica sleeve only, the principal path for sublimation appears to be at the ends of the mica sleeve, particularly in the region of the mica-sleeve/tungsten hot-shoe (see Figure 14). However, the application of an oxide-fiber shroud significantly reduces the conductance at the ends of the sleeve by virtue of the tortuous path afforded by the 6 to 7 layers of fibers.

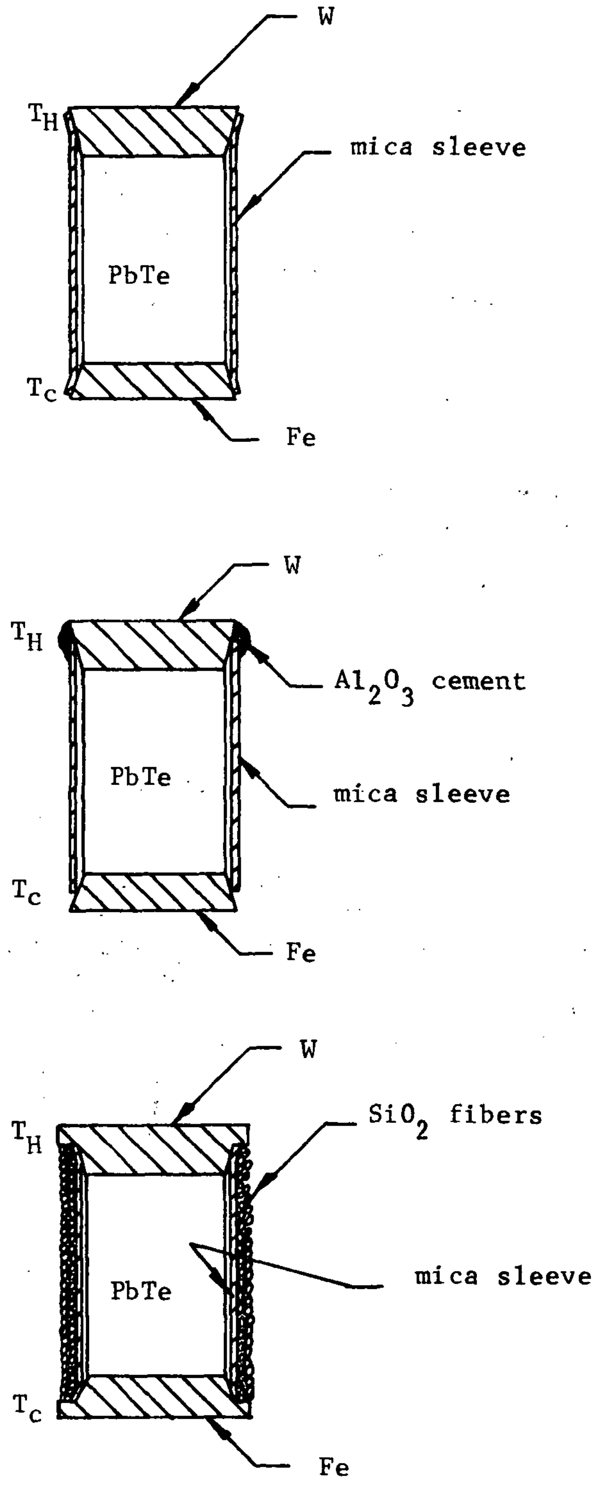

FIGURE 14. BARRIER SCHEMES FOR SUPPRESSING SUBLIMATION OF THERMOELECTRIC MATERIALS

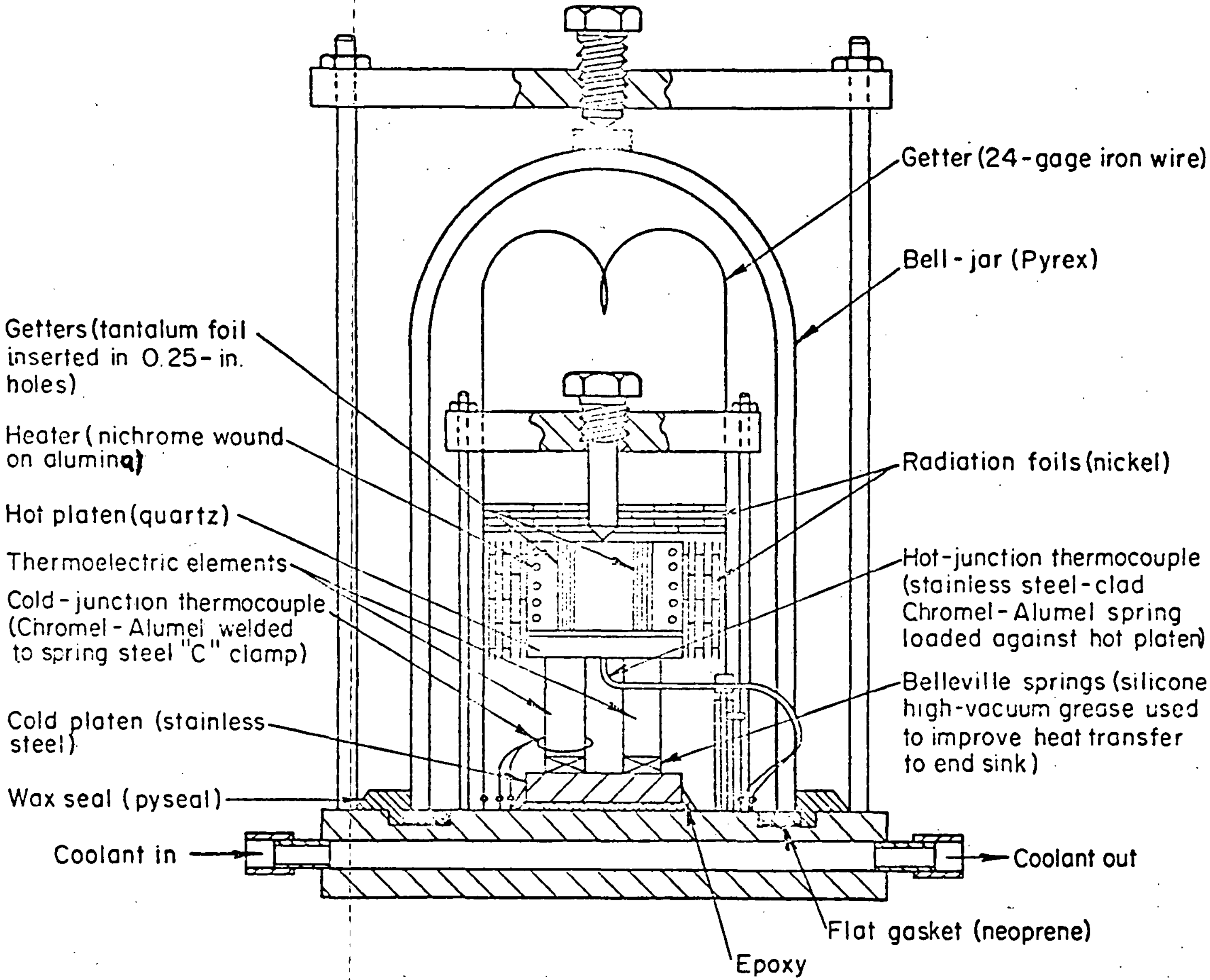

FIGURE 15. AMPOULE TEST FIXTURE (REVISED DESIGN)

of approximately 450 hr. At the completion of the in-gradient tests, the sublimation barrier is removed and the specimen is weighed again in order to determine the weight loss. The results of these in gradient tests are discussed below.

Experimental Results

The results of the above in-gradient tests are summarized in Table 4. The experimental results indicate that a three-fold reduction in the sublimation rate (relative to a mica barrier alone) can be realized by applying an Al_2O_3 shroud at the mica-sleeve/tungsten hot-shoe interface (see specimen numbers SB-71-1 and -4). Even more significant, a 12- to 50-fold reduction in the sublimation rate (relative to a mica barrier alone) can be realized by applying a shroud of 6-7 layers of oxide fibers (see specimen numbers SB-71-1, -3, -5). The outstanding barrier effectiveness for the oxide-fiber barrier scheme was confirmed by repeating the experiment (see Specimen Number SB-71-5).

The above results indicate that, based on percent weight loss, the oxide-fiber-shroud-over-mica-sleeve barrier scheme is far superior to the other barrier schemes investigated. An analysis was also performed to translate "percent weight loss" to "increase in electrical resistance" of the thermoelectric couple. For the present experimental conditions (0.76-cm-diameter x 1.5-cm-long thermoelements operating between 527 C and 25 to 35 C), the 0.04 percent weight loss in specimen number SB-71-5 corresponds to a total element resistance increase of less than 0.2 percent. Hence, one could expect less than 0.2 percent decrease in output power* of the p-type PbTe leg after operating for approximately 450 hours in vacuum. This rate of resistance increase due to sublimation would, of course, be further reduced if the same oxide-fiber enclosed p-type PbTe element were operated in an inert atmosphere in place of vacuum.

Posttest examination of the above specimens was performed using Seebeck coefficient traverse measurements.[9] These measurements provide longitudinal Seebeck coeffcient profiles both at the surface of the specimen and at the centerline of the specimen. The results of these traverse measurements revealed that there was no apparent preferential sublimation of Te from the 2p PbTe. Hence, it can be inferred that observed weight losses can be interpreted as being bulk PbTe loss in contrast to preferential loss of the property-controlling dopants (excess Te in the present case).

---

* Due to erosion of thermoelectric element by sublimation.

TABLE 4. SUMMARY OF WEIGHT LOSS FOR 2p-PbTe ELEMENTS OPERATED IN VACUUM AND INVOLVING SELECTED SUBLIMATION BARRIER SCHEMES

Specimen Number	Barrier Scheme	Hours on Test	Hot-Junction Temperature, C	Weight Loss, percent
SB-71-1	Mica sleeve	445	520-527	0.48
SB-71-2	No barrier	25	520-524	2.75
SB-71-3	Oxide-fiber shroud over mica sleeve	455	522-529	0.01
SB-71-4	Mica sleeve with Al_2O_3 cement at mica/W interface	454	526-531	0.18
SB-71-5	Oxide-fiber shroud over mica sleeve	454	528-533	0.04

REFERENCES

(1) Kinney, R. D., "The Evaporative Erosion of Thermoelectric Elements in Some Thermoelectric Generators", Report SC-RR-70-534, Sandia Laboratories (September, 1970).

(2) Eggers, P. E., Mueller, J. J., "Oxygen-Enhanced Sublimation of Type PbTe Thermoelectric Materials", Proceedings of the 6th IECEC Conference, Boston, Massachusetts (August, 1971).

(3) Powell, A. H., "Compression Springs for Long Time Operation in Vacuum at 1000 F", Topical Report GESP-345 (December, 1969).

(4) Kortier, W. E., Mueller, J. J., Eggers, P. E., and Freas, D. G., "A Research and Development Program for Segmenting Silicon Gernamium and Lead Telluride Thermoelectric Materials", Final Report, Contract NAS5-10185 (December 16, 1966).

(5) Eggers, P. E., and Mueller, J. J., "An Advanced Thermoelectric Life Test and Evaluation Study", Final Report, Contract NAS5-14097 (September 28, 1968).

(6) Eggers, P. E., "An Advanced Thermoelectric Life Test and Evaluation Study", Final Report, Contract NAS5-11644 (June 30, 1969).

(7) Eggers, P. E., "Study of Test and Measurement Standardization Techniques Associated with Thermoelectric Materials", Contract NAS5-21099 (November, 1969 to August, 1970).

(8) Powell, A. H., "Compression Springs for Long Time Operation in Vacuum at 1000 F", Topical Report GESP-345 (December, 1969).

(9) Mueller, J. J., et al, "Seebeck Voltage Probe for Examination of Thermoelectric Elements", 1968 IECEC Conference Proceedings.

(10) For OFFOPT correlation study see Eggers, P. E., "Performance of Life Tests and Efficiency Measurements for Thermoelectric Couples at Constant Thermal Input Power", ASME Technical Publication Number 69-WA/Ener-14$_3$ (1969)

(11) For TRUMP correlation study compare results in Figure B-1 with results reported in "An Advanced Thermoelectric Life Test and Evaluation Study", Final Report under Contract NAS5-10497, page 73-74 (September, 1968)

APPENDIX A

USERS MANUAL FOR TRANRTG RTG TRANSIENT ANALYSIS COMPUTER PROGRAM

<ins>Note</ins>: The input data forms contained in this appendix organize the input data into functional groups. These forms also provide a convenient format for data compilation since each input parameter is briefly described in the adjacent column titled "Description". Note that a number of the control data values have been specified previously on pages A-4 and A-8 and should not be altered. The specified data values together with the user-supplied data should be keypunched according to the format specified in these data forms.

ANALYTICAL EQUATIONS FOR TRANRTG

1. RTG Design-Optimization Equations (GESPGN)

The equations for the RTG design optimization are contained in the NASA-Goddard final report, "The Analysis and Design of a High-Temperature Thermoelectric Conversion Device", BAT-5-6397-2, classified Confidential-Defense Information, NAS 5-3697 (1965); also Eggers, P. E., "An Advanced Thermoelectric Life Test and Evaluation Study", NASA Contract No. NAS 5-10497, Final Report, September, 1968.

2. Thermoelectric-Analysis Equations (OFFOPT)

The equations for the thermoelectric analyses are described in the report "Progress on the Development of Segmented PbTe-Bi_xTe Thermoelectric Modules", AEC Contract W-7405-eng-92, BMI Report No. BMI-1794 (January, 1967). A more detailed discussion can be found in "Development of an Analysis Technique for Predicting the Operating Characteristics of Thermoelectric Heat Engines", R. E. Best, The Ohio State University, 1970 (thesis).

3. Heat-Transfer Equations (TRUMP)

The equations for the steady-state and transient heat-transfer analyses are reported in "TRUMP Computer Program" by A. L. Edwards, Lawrence Radiation Laboratory Report Number UCRL-14754 Revision II (1969).

4. Supplementary Equations

Additional equations used in the TRANRTG computer program but not described in the above references include:

(a) Sublimation Rate Equation. The postulated equation, described on page A-4, permits the user to supply empirically derived sublimation rates for the thermoelements in terms of coefficients and exponents for an exponential model of the form:

$$y = Ae^{BT}.$$

This model, in general, provides a good fit to empirically derived evaporation rates for thermoelectric materials.

(b) Radioisotope Decay. This equation is based on the relationship

$$Q = Q_o e^{-\lambda t}$$

where

Q_o = initial thermal power

λ = disintegration constant = $\frac{.693}{\text{half life}}$

t = time (same units as half life) .

FORTRAN FIXED 10 DIGIT DECIMAL DATA

DECK NO.______ PROGRAMMER______ DATE______ PAGE 1 of______ JOB NO.______

	NUMBER	IDENTIFICATION	DESCRIPTION DO NOT KEY PUNCH
1			Cross-sectional area of n-leg (cm^2)
13			Cross-sectional area of p-leg (cm^2)
25			Beginning-of-life thermopile cold junction temperature (K)
37			Beginning-of-life thermopile hot junction temperature (K)
49		73 80	Length of thermoelectric elements (cm)
61		B L O C K 1 - 1	Temperature difference between thermopile cold junction temperature and fin root temperature (K)
1			Temperature difference between thermopile hot junction temperature and heat source surface temperature (K)
13			Power density multiplying factor (set to 1.0)
25			Ratio of external load to thermopile internal resistance
37			
49		73 80	
61		B L O C K 1 - 2	
1			
13			
25			
37			
49		73 80	
61			
1			
13			
25			
37			
49		73 80	
61			

FORTRAN FIXED 10 DIGIT DECIMAL DATA

DECK NO. ______ PROGRAMMER ______ DATE ______ PAGE 2 of ______ JOB NO. ______

Col.	NUMBER	IDENTIFICATION	DESCRIPTION DO NOT KEY PUNCH
1			Polynominal coefficients for p-leg resistivity - coefficient 1
13			(units of ohm-cm) - coefficient 2
25			- coefficient 3
37			- coefficient 4
49		73 80	- coefficient 5
61		BLOCK2 -1	- coefficient 6
1			- coefficient 7
13			- coefficient 8
25			Polynominal coefficients for n-leg resistivity - coefficient 1
37			(units of ohm-cm) - coefficient 2
49		73 80	- coefficient 3
61		BLOCK2 -2	- coefficient 4
1			- coefficient 5
13			- coefficient 6
25			- coefficient 7
37			- coefficient 8
49		73 80	Polynominal coefficients for p-leg thermal - coefficient 1
61		BLOCK2 -3	conductivity (units of watts/cm-C) - coefficient 2
1			- coefficient 3
13			- coefficient 4
25			- coefficient 5
37			- coefficient 6
49		73 80	- coefficient 7
61		BLOCK2 -4	- coefficient 8

FORTRAN FIXED 10 DIGIT DECIMAL DATA

DECK NO.______ PROGRAMMER ______ DATE ______ PAGE 3 of ______ JOB NO. ______

	NUMBER	IDENTIFICATION	DESCRIPTION DO NOT KEY PUNCH	
1			Polynominal coefficients for n-leg thermal	- coefficient 1
13			conductivity (units of watts/cm-C)	- coefficient 2
25				- coefficient 3
37				- coefficient 4
49		73 80		- coefficient 5
61		B L O C K 2 - 5		- coefficient 6
1				- coefficient 7
13				- coefficient 8
25			Polynominal coefficients for p-leg Seebeck	- coefficient 1
37			coefficient (units of volts/C)	- coefficient 2
49		73 80		- coefficient 3
61		B L O C K 2 - 6		- coefficient 4
1				- coefficient 5
13				- coefficient 6
25				- coefficient 7
37				- coefficient 8
49		73 80	Polynominal coefficients for n-leg Seebeck	- coefficient 1
61		B L O C K 2 - 7	coefficient (unit of volts/C)	- coefficient 2
1				- coefficient 3
13				- coefficient 4
25				- coefficient 5
37				- coefficient 6
49		73 80		- coefficient 7
61		B L 0 C K 2 - 8		- coefficient 8

FORTRAN FIXED 10 DIGIT DECIMAL DATA

DECK NO._____ PROGRAMMER_____ DATE_____ PAGE 4 of_____ JOB NO._____

Col.	NUMBER	IDENTIFICATION	DESCRIPTION DO NOT KEY PUNCH
1			Contact resistivity of p-leg hot junction ($ohm\text{-}cm^2$)
13	0.0		Contact resistivity of p-leg intermediate junction ($ohm\text{-}cm^2$)
25			Contact resistivity of p-leg cold junction ($ohm\text{-}cm^2$)
37			Contact resistivity of n-leg hot junction ($ohm\text{-}cm^2$)
49	0.0	73 80	Contact resistivity of n-leg intermediate junction ($ohm\text{-}cm^2$)
61		BLOCK 3 - 1	Contact resistivity of n-leg cold junction ($ohm\text{-}cm^2$)
1	0.10		Initial current for I-V sweep (amps)
13	0.50		Large step size for current iterations (amps)
25	0.05		Small step size for current iterations (amps)
37	0.05		Tolerance for element length iterations (cm)
49	.00020	73 80	Step size for first stage of element during iterations (cm)
61		BLOCK 3 - 2	Exponents and intercepts for A for N leg segment
1			vaporization rates of B for N leg segment
13			thermoelectric elements A for P leg segment
25			according to the relationship: B for P leg segment
37	0.0		$y = Ae^{BT}$ A for N leg-hot segment
49	0.0	73 80	where y is in units of
61	0.0	BLOCK 3 - 3	($grams/cm^2$ hr)
1	0.0		
13			Density of n-leg hot segment ($grams/cm^3$)
25			Density of p-leg hot segment ($grams/cm^3$)
37			Radiation heat transfer view factor from element
49		73 80	
61		BLOCK 3 - 4	

FORTRAN FIXED 10 DIGIT DECIMAL DATA

DECK NO. ______ PROGRAMMER ______ DATE ______ PAGE 5 of ____ JOB NO. ______

Col.	NUMBER	IDENTIFICATION	DESCRIPTION DO NOT KEY PUNCH
1			Thermoelement geometry factor; if 1.0, rectangular elements; if 0.0, circular elements
13			Temperature exponent of contact resistivity, c, where $\rho_c \propto T^c$
25			Tolerance function for assumed thermopile temperature difference, C
37			Tolerance function for assumed radiator temperature, C
49		73 80	Tolerance function for assumed cold junction temperature, C
61		B L O C K 3 - 5	Tolerance function for assumed hot junction temperature, C
1			Half life of radioisotope (years)
13			Density of n-leg cold segment (grams/cm^3)
25			Density of p-leg cold segment (grams/cm^3)
37			
49		73 80	
61		B L O C K 3 - 6	
1			
13			
25			
37			
49		73 80	
61			
1			
13			
25			
37			
49		73 80	
61			

FORTRAN FIXED 10 DIGIT DECIMAL DATA

DECK NO. ______ PROGRAMMER ______ DATE 6 ______ PAGE ____ of ____ JOB NO. ______

	NUMBER	IDENTIFICATION	DESCRIPTION DO NOT KEY PUNCH
1			Permanent Data Set 1
13			(supplied with computer program)
25			
37			
49		73 80	
61		B L O C K 4	
1			
13			
25			
37			
49		73 80	
61			
1			
13			
25			
37			
49		73 80	
61			
1			
13			
25			
37			
49		73 80	
61			

FORTRAN FIXED 10 DIGIT DECIMAL DATA

DECK NO.____ PROGRAMMER____ DATE____ PAGE 7 of ____ JOB NO.____

Col.	NUMBER	IDENTIFICATION	DESCRIPTION DO NOT KEY PUNCH
1		Radiator Fin Inputs Note: Last three inputs on this card required only if data other than that in library are desired.	Radiator material I.D. number(1)* (Col. 1) and material name (e.g. beryllium)
13			Number of radiator fins $(2 \leq N \leq 8)$
25			Radiator fin emissivity
37			Fin-length parameter,(2) $\emptyset(cm^2 - °K^4/W)$
49		73 … 80	Fin-thickness parameter, $\varphi(cm^3 - °K^5/W^2)^{1/2}$
61		B L O C K 5 - 1	Fin-weight parameter, $\mu(cm^2 - lb - °K^9/W^3)^{1/2}$
1		Thermopile Inputs	Thermoelectric material (e.g., PbTe, GeSi, etc.)
13			Thermoelectric hardware material (e.g., S.S. 304)
25			Thermoelectric hot-shoe material (e.g., tungsten, iron, etc.)
37			Thermoelectric cold-shoe material (e.g., tungsten, iron, etc.)
49		73 … 80	Interelement thermal and electrical insulation material (e.g., mica)
61		B L O C K 5 - 2	Module cladding material (e.g., S.S. 304)
1			Thermoelectric element length assumed (cm)
13	1		
25	1		
37			Number of modules(3)
49		73 … 80	
61		B L O C K 5 - 3	
1			Length-to-area ratio of Phase I n-element (cm^{-1})
13			Length-to-area ratio of Phase I p-element (cm^{-1})
25	0.0		
37	0.0		
49	0.0	73 … 80	
61	0.0	B L O C K 5 - 4	

* Superscript numbers refer to explanatory notes at end of Appendix A.

FORTRAN FIXED 10 DIGIT DECIMAL DATA

DECK NO. ______ PROGRAMMER ______ DATE ______ PAGE 8 of ______ JOB NO. ______

Col.	NUMBER	IDENTIFICATION	DESCRIPTION DO NOT KEY PUNCH
1			Density of Phase I n-type segment (lb/cc)
13			" " " I p-type " "
25	0.0		
37	0.0		
49	0.0	73 80	
61	0.0	BLOCK 5-5	
1	1.0		Number of thermoelectric element segments
13			Element distribution in module width(4) (0 - odd or even, 1 - even only)
25			Density of thermoelectric hardware (hot and cold platens, etc.) (lb/cc)
37			Density of module cladding material (lb/cc)
49		73 80	Density of thermoelectric shoe material (lb/cc)
61		BLOCK 5-6	Density of thermal and electrical insulation between elements (lb/cc)
1			Thermoelectric hardware thickness in conductive mode (cm)
13			Thermoelectric hardware thickness in radiative mode (cm)
25			Radiation gap between heat source and module (cm)
37			Thickness of element shoes (cm)
49		73 80	Thickness of module periphery material (cm)
61		BLOCK 5-7	Thickness of module peripheral gap for radiation-loss analysis (cm)
1			
13			
25			
37			
49		73 80	
61			

FORTRAN FIXED 10 DIGIT DECIMAL DATA

DECK NO.______ PROGRAMMER______ DATE______ PAGE 9 of______ JOB NO.______

Col.	NUMBER	IDENTIFICATION	DESCRIPTION DO NOT KEY PUNCH
1			Thickness of thermal and electrical insulation between elements (cm)
13			Effective thermal conductivity of module periphery (watts/cm/°C)
25			Effective thermal conductivity of thermal and electrical insulation
37			(watts/cm/°C)
49		73 80	
61		B L O C K 5 - 8	
1		Fuel-Form Impact Cladding Inputs	Fuel-form cladding material (e.g., Inconel 716)
13			Inner-liner cladding material (e.g., tantalum)
25			Outer-shell cladding material (e.g., molybdenum)
37			Fuel-tube material (e.g., molybdenum)
49		73 80	Toughness parameter of cladding(5) (lb/cm^2)
61		B L O C K 5 - 9	Thickness of inner-liner cladding (cm)
1			Thickness of outer-shell cladding (cm)
13			Thickness of fuel tube (cm)
25			Density of fuel-form cladding (lb/cc)
37			Density of inner-liner cladding (lb/cc)
49		73 80	Density of outer-shell cladding (lb/cc)
61		B L O C K 5-10	Density of fuel tube (lb/cc)
1		Fuel-Form Inputs	Fuel-form material (e.g., plutonium)
13			Fuel-block material (e.g., graphite)
25			Fuel-form power density(6) (watts/cc)
37			Fuel-pin density in close-packing matrix(7) (decimal)
49		73 80	
61		B L O C K 5-11	Fuel-pin array option* (0 - locus of all fuel-pin centers is a circle; 1 - close packing of fuel pins)

* Kortier, W. E., "An Advanced Thermoelectric Component Program Final Summary Report", February 18, 1966, page 6, NAS5-9160.

FORTRAN FIXED 10 DIGIT DECIMAL DATA

DECK NO. ______ PROGRAMMER ______ DATE ______ PAGE 10 of ______ JOB NO. ______

Column	NUMBER	IDENTIFICATION	DESCRIPTION DO NOT KEY PUNCH
1			Fuel pin - fuel tube separation[8] (cm)
13			Fuel-pin separation (cm)
25			Number of fuel pins
37			"Effective" surface-power-density available for module[9] (watts/cm^2)
49		73 80	Heat-transfer mode between heat source and module (1 - conductive, 2 - radiative)
61		Block 5-12	Density of fuel block (lb/cc)
1			Density of fuel form[10] (lb/cc)
13			Density of fuel pin (lb/cc)
25			Limiting aspect ratio of fuel form
37			Limiting aspect ratio of fuel pin
49		73 80	
61		Block 5-13	
1		Heat-Source Support Inputs	Heat-source-support material for ends (e.g., Min-K 2000)
13			Heat-source-support material for radial portion (e.g., Min-K 2000)
25			Thermal insulation material for ends
37			Thermal insulation material for radial portion
49		73 80	Absolute end support option (0 - all support on ends; 1 - some support on radial portion)
61		Block 5-14	Absolute radial support option (0 - all support on radial portion) 1 - some support on ends)
1			Elastic modulus[11] (compression) of end heat-source support (lb/cm^2)
13			Elastic modulus (compression) of radial heat-source support (lb/cm^2)
25			Elastic modulus (shear) of end heat-source support (lb/cm^2)
37			Elastic modulus (shear) of radial heat-source support (lb/cm^2)
49		73 80	Neglect of heat-source-support end-deflection[12]
61		Block 5-15	(0 - deflection controls generator length; 1 - generator length independent of deflection)

FORTRAN FIXED 10 DIGIT DECIMAL DATA

DECK NO. ______ PROGRAMMER ______ DATE ______ PAGE 11 of ______ JOB NO. ______

Column	NUMBER	IDENTIFICATION	DESCRIPTION DO NOT KEY PUNCH
1			Heat-source-support foil separation on end support (cm)
13			Heat-source-support foil separation on radial support (cm)
25			End-insulation-foil separation (cm)
37			Radial-insulation-foil separation (cm)
49		73 80	Thermal conductivity of end heat-source support (watts/cm/°C)
61		Block 5-16	Thermal conductivity of radial heat-source support (watts/cm/°C)
1			Thermal conductivity of end insulation (watts/cm/°C)
13			Thermal conductivity of radial insulation (watts/cm/°C)
25			Density of the end heat-source support (lb/cc)
37			Density of the radial heat-source support (lb/cc)
49		73 80	Density of the end insulation (lb/cc)
61		Block 5-17	Density of the radial insulation (lb/cc)
1			Maximum tolerable deflection of end heat-source support(13) (cm)
13			Maximum tolerable deflection of radial heat-source support(13) (cm)
25			
37			
49		73 80	
61		Block 5-18	
1		Generator Shell Inputs	Generator shell material (e.g., beryllium)
13			Final overall generator length (cm)
25			Normal increment step-size for generator length (cm)
37			Initial overall generator length (cm)
49		73 80	Density of generator shell (lb/cc)
61		Block 5-19	Thickness of ablator on end (cm)

FORTRAN FIXED 10 DIGIT DECIMAL DATA

DECK NO.______ PROGRAMMER______ DATE______ PAGE 12 of____ JOB NO.______

Col.	NUMBER	IDENTIFICATION	DESCRIPTION DO NOT KEY PUNCH
1			Thickness of ablator on radial portion (cm)
13			Thermal conductivity of generator shell (watts/cm/°C)
25			Limiting aspect ratio of generator envelope
37			Limiting aspect ratio of generator shell
49		73 80	Percent of total heat-dump capability of generator ends(14) (decimal)
61		Block 5-20	Thickness of radiator shell
1		RTG Analysis Computation Options (Note: See end of Appendix I for description of these options)	Thermoelectric-array computation sequence (1,2,3)(19)
13			Generator-length computation sequence (0,1)
25			Thermoelectric-element-length computation sequence (0,-1)
37			Fuel-form geometry option (0,1)
49		73 80	Heat-source-support computation option (-1,0,1)
61		Block 5-21	End-insulation computation option (-1,0)
1			Insulation and heat-source-support option (0,1)
13			Insulation and heat-source-support material option (0,1)
25			Print option for output data(15) (0 - abstract, 1 - detailed, 2 - super-detailed)
37			Plot option (1 - plot component weights vs generator length;
49		73 80	2 - plot component weights vs radiator temperature; 3 - no plot)
61		Block 5-22	Output format option(15) (0 - abstract, 1 - detailed)
1		Temperatures(16)	Temperature of thermoelement cold junction (K)
13			Temperature at cold end of insulation (K)
25			Temperature of thermoelement hot junction (K)
37			Temperature at hot end of insulation (K)
49		73 80	Temperature at heat-source surface (that surface which is adjacent to module) (K)
61		Block 5-23	Temperature of radiator fin and generator shell (K)

FORTRAN FIXED 10 DIGIT DECIMAL DATA

DECK NO._____ PROGRAMMER_____ DATE_____ PAGE 13 of_____ JOB NO._____

	NUMBER	IDENTIFICATION	DESCRIPTION DO NOT KEY PUNCH
1		General Design Inputs	Assumed engineering efficiency[17] (decimal form)
13			Minimum thermoelectric element length to be considered by generator[18] (cm)
25			Maximum element length to be considered by generator[18] (cm)
37			"g"-loading axially (dimensionless)
49		73 80	"g"-loading radially (dimensionless)
61		Block 5-24	Generator power level (watts(e))
1			Impact velocity of heat source[5] (cm/sec)
13			
25	1		Data set index for component weight versus cold-junction temperature
37			option
49		73 80	
61		Block 5-25	
1			
13			
25			
37			
49		73 80	
61			
1			
13			
25			
37			
49		73 80	
61			

FORTRAN FIXED 10 DIGIT DECIMAL DATA

DECK NO. ______ PROGRAMMER ______ DATE ______ PAGE 14 of ___ JOB NO. ______

	NUMBER	IDENTIFICATION	DESCRIPTION DO NOT KEY PUNCH
1			Effective density of heat source (g/cm^3)
13			Effective specific heat of heat source (cal/g-K)
25			Effective thermal conductivity of heat source (cal/sec-cm-K)
37			Melting point of heat source (K)
49		73 80	Latent heat of fusion heat source (cal/g)
61		Block 6-1	
1			Effective density of thermal insulation (g/cm^3)
13			Effective specific heat of thermal insulation (cal/g-K)
25			Effective thermal conductivity of thermal insulation (cal/sec-cm-K)
37			Melting point of thermal insulation (K)
49		73 80	Latent heat of fusion thermal insulation (cal/g)
61		Block 6-2	
1			Effective density of RTG fins and shell (g/cm^3)
13			Effective specific heat of RTG fins and shell (cal/g-K)
25			Effective thermal conductivity of RTG fins and shell (cal/sec-cm-K)
37			Melting point of RTG fins and shell (K)
49		73 80	Latent heat of fusion of RTG fins and shell (cal/g)
61		Block 6·3	
1			Effective density of thermoelements (g/cm^3)
13			Effective specific heat of thermoelements (cal/g-K)
25			Blank
37			Melting point of thermoelements (K)
49		73 80	Latent heat of fusion of thermoelements (cal/g)
61		Block 6-4	

FORTRAN FIXED 10 DIGIT DECIMAL DATA

DECK NO. ________ PROGRAMMER ________ DATE ________ PAGE 16 of ____ JOB NO. ________

Col.	NUMBER	IDENTIFICATION	DESCRIPTION DO NOT KEY PUNCH		
1		Transient data (20)	Case number (index) for transient analyses (2., 3., etc.)		
13			Elapsed time since last data set (hr)		
25			Sublimation factor; if 0.0, sublimation, if 1.0, no sublimation		
37			Minimum temperature at which sublimation will be significant.(K)		
49		73 ... 80	Coefficients for thermoelectric	Sect. I:	p-leg resistivity
61		B L O C K 8 - 1	properties; used to simulate		n-leg resistivity
1			change in thermoelectric		p-leg th. cond.
13			properties according to		n-leg th. cond.
25			four sections of legs of		p-leg Seebeck coefficient
37			equal temperature difference		n-leg Seebeck coefficient
49		73 ... 80	Section I - hot section	Sect. II:	p-leg resistivity
61		B L O C K 8 - 2	Section II - medium-hot section		n-leg resistivity
1			Section III - medium-cold section		p-leg th. cond.
13			Section IV - cold section		n-leg th. cond.
25			(unitless coefficients)		p-leg Seebeck coefficient
37			If no thermoelectric material		n-leg Seebeck coefficient
49		73 ... 80	degradation, enter 1.0 in	Sect. III:	p-leg resistivity
61		B L O C K 8 - 3	all fields of Sections I-IV		n-leg resistivity
1			These coefficients are based		p-leg th. cond.
13			on either estimated or		n-leg th. cond.
25			measured normalized property		p-leg Seebeck coefficient
37			changes.		n-leg Seebeck coefficient
49		73 ... 80		Sect. IV:	p-leg resistivity
61		B L O C K 8 - 4			n-leg resistivity

FORTRAN FIXED 10 DIGIT DECIMAL DATA

DECK NO. ______ PROGRAMMER ______ DATE ______ PAGE 15 ______ of ______ JOB NO. ______

	NUMBER	IDENTIFICATION	DESCRIPTION DO NOT KEY PUNCH
1			Permanent Data Set 2
13			(supplied with computer program)
25			
37			
49		73 80	
61		BLOCK7	
1			
13			
25			
37			
49		73 80	
61			
1			
13			
25			
37			
49		73 80	
61			
1			
13			
25			
37			
49		73 80	
61			

FORTRAN FIXED 10 DIGIT DECIMAL DATA

DECK NO. ______ PROGRAMMER ______ DATE ______ PAGE 17 of ______ JOB NO. ______

Col.	NUMBER	IDENTIFICATION	DESCRIPTION DO NOT KEY PUNCH	
1			Coefficients (continued) Sect. IV:	p-leg th. cond.
13				n-leg th. cond.
25				p-leg Seebeck coefficient
37				n-leg Seebeck coefficient
49		73 80	Contact resistivity coefficients	p-leg, hot junction
61		B L O C K 8 - 5	to simulate increase or	p-leg, intermediate junction
1			decrease of contact	p-leg, cold junction
13			resistivity with time	n-leg, hot junction
25			(unitless)	n-leg, intermediate junction
37				n-leg, cold junction
49		73 80	Vaporization rate	p-leg, hot segment
61		B L O C K 8 - 6	coefficients to simulate	n-leg, hot segment
1			change in rate due to, e.g., change	p-leg, cold segment
13			in cover gas pressure (unitless)	n-leg, cold segment
25			Coefficient to simulate change in load resistance (unitless)	
37			Coefficient to simulate change in radiator emittance (unitless)	
49		73 80	Incident solar heat flux or planetary	Node 11, 12
61		B L O C K 8 - 7	albedo; adjust heat flux	Node 9, 10
1			to correspond to appropriate	Node 35
13			angle of incidence	Node 36
25			(watts/cm2)	Node 37
37				Node 38
49		73 80	Total elapsed time (hr)	
61		B L O C K 8 - 8	Printout interval for absolute transient condition[21] (seconds)	

FORTRAN FIXED 10 DIGIT DECIMAL DATA

DECK NO.______ PROGRAMMER______ DATE______ PAGE 18 of______ JOB NO.______

	NUMBER	IDENTIFICATION	DESCRIPTION DO NOT KEY PUNCH
1			Absolute transient factor[22] (steady state = 0, transient = 1)
13			RTG boundary temperature (K)[23]
25			Convection and conduction heat transfer coefficient for radiator[23] (cal/sec cm^2 C)
37			Start-up option[24] (0-No, 1-Yes)
49		73 80	Initial RTG temperature for start-up transient analysis (K)
61			Coefficient to simulate change in k of thermal insulation (unitless)
1			Maximum time for transient analysis
13			If set = 1, last transient data set for given subproblem
25			
37			
49		73 80	
61			
1			
13			
25			
37			
49		73 80	
61			
1			
13			
25			
37			
49		73 80	
61			

Explanatory Notes on Input Data

(1) Radiator-Material Designation

The following radiator-material numbering code may be used to extract the radiator fin parameters from the input-data library:

Radiator Material I. D. Number	Radiator Material
1	Magnesium
2	Beryllium
3	Magnesium M1A
4	Magnesium HM21-T8
5	Aluminum A356-T6

(2) Fin Parameters

If materials other than the above are desired, see reference* for details of parameter calculation.

(3) Selection of Module Number

The selection of the number of modules is a tradeoff between module peripheral losses and desired number of fins. For maximum utilization of radiator fins, the number of modules should match the number and position of the fins. Therefore, this selection will be subject to the selection of the number of fins discussed.

(4) Thermoelectric-Array Option

The choice of module-width array is affected by the requirements imposed by equipment used in the vicinity of the generator. For example, for magnetometers, extraneous fields produced by current-carrying wires must be arranged so that they are self cancelling. This is achieved by an array with equal numbers of n- and p-elements across the width of the module, and this can be introduced into the program by means of the input value set equal to 1.0.

---

* Burian, R. J., et al, "A Design Procedure for the Weight Optimization of Straight Finned Radiators", NASA Technical Note TN D-3489 (August, 1966).

(5) Toughness Parameter and Impact Velocity

This parameter is used in the cladding-analyses subroutine of the program. The selection of this term is discussed in the final report of NASA Contract NAS5-3697, page 25. Also in this reference appears a discussion of the impact velocity and how the cladding analyses establish a cladding thickness sufficient for intact impact with an unyielding surface.

(6) Fuel-Form Power Density

This power density is usually found in the properties table of a candidate fuel form. However, when radioisotope gas must be accommodated by void space, the fuel-form power density is reduced to an effective power density. This power density is used to determine the volume the fuel form will occupy, including the void volume.

(7) Fuel-Pin Packing Density

This parameter defines the packing density of the fuel pins in the fuel-block matrix. The maximum packing fraction is about 70 percent and will have to be determined prior to the computer run. This number, when divided into the total cross-sectional area of the fuel pins, will give the total cross-sectional area of the fuel-form cross section. The value is used when an undefined array is specified.

(8) Separation Between the Fuel Pin-Fuel Tube and Between Fuel Pins

This input permits the operator to choose the fuel-block thickness between a fuel pin and the fuel tube which supports the fuel block plus fuel pins. This only applies to the symmetric fuel-pin array which is selected by the input value for FPA, the fuel-pin-array option.

The separation between fuel pins along a line connecting the fuel-pin centers allows the packing density to be controlled. Note that the fuel block is optional in the case of radiation heat transfer. In this case, the fuel pins would be supported by a frame whose weight would be included under the heading of the fuel block.

(9) Heat-Source-Surface Power Density

The heat-source-surface power density is selected on the basis of maximum-power-density capability. This value is found from two-dimensional heat-flow considerations of the fuel form, fuel block, cladding, and fuel-tube composite. The term is then used in the computer to determine whether the designed thermoelectric module requires a surface power density greater than that practical for a particular heat-source design. A surface-power-density deficiency will result in an escalation of the heat-source surface temperature which will increase parasitic heat losses through the insulation and heat-source support.

(10) Fuel-Form Density

The fuel-form density may be expressed as an effective value if void volumes are incorporated into the fuel form. For example, if a fuel requires an additional 100 percent void volume due to fission radioisotope-decay gas release, then the effective fuel-form density, RHOFF, would be one-half the actual fuel-form density for the weight calculation.

(11) Modulus of Elasticity for Heat-Source Support

The compressive- and shear-modulus inputs are necessary for the determination of heat-source support required for a maximum allowed deflection. The values will often be supplied with homogeneous materials. However, for more complex support structures, such as honeycomb, special data reports must be consulted. Since heat-source support is a basic necessity, the support medium may have to be designed for a required modulus.

(12) Neglect of Heat-Source-Support End Deflection

This option permits the code to consider or ignore longer generators when a deficiency of end-support bearing-area exists. Longer generators are attended by decreasing end areas, which serves to increase the bearing-area deficiency.

(13) Maximum Tolerable Deflections

The module, heat source, or support may be limited in deflection because of preservation of electrical or thermal contacts of the thermoelectrics, excessive shear forces on thermoelectrics or heat-source support, or increase in heat transfer through heat-source support, or insulation due to reduction in heat path.

(14) Heat Dissipation by Generator Ends

The particular mission of a generator may allow all, part, or none of the end area of the generator shell to dissipate heat. This may be introduced into the program by specifying the percentage of the total dissipative capability available for heat dump.

(15) Output Options

The print option for output data controls the frequency of the display of output data, e.g., the user may choose to (1) print the calculated data after a change in each component (superdetailed mode), (2) print the calculated data after each component has been optimized (detailed), and (3) print only the optimum generator-design case (abstract).

The output-format operation permits the user to specify (1) an output format containing all dimensions, weights, etc. (detailed) or (2) an output format containing only the principal parameters (abstract). A description of both types of output format is given in Appendix B.

(16) Generator Profile Temperatures

The temperatures of the cold junction of the thermoelectrics, cold junction of the insulation, and the radiator surface may all be specified independently to accommodate the temperature differentials present in the heat path for the thermoelectric cold junction to the radiator surface. The same procedure is used at the hot junction.

(17) Generator Profile Temperatures

This program is designed to construct mathematically a generator based on assumed thermoelectric and engineering efficiencies. Therefore, the operator must select a practical value of engineering efficiency for the program. The program will analyze and iterate on engineering efficiency until a heat balance is achieved. Thus, the proper selection of this parameter will greatly reduce the computer run time.

(18) Element-Length Limits

These limits are imposed to avoid impractical element shapes and sizes due to the element-length iterations taking place in the program. The limits may be based on fabricability or insulation capability, since insulation thickness and heat-source-support thickness follows the element length.

(19) RTG Analysis Computation Options

(a) Thermoelectric-array computation sequence

1 - Limited by heat-source diameter
2 - Limited by heat-source length
3 - Investigates Cases 1 and 2

Geometry of module based on geometry of heat sources

(b) Generator length computation sequence

0 - Iterate using normal increments
1 - Iterate using large increments and then small increments

(c) Thermoelectric-element-length computation sequence

0 - Element length is fixed
1 - Element length is varied in order to trade off thermoelectric weight versus other generator components (viz, heat source, insulation, shell, etc.)

(d) Fuel-form geometry option

0 - Right-cylindrical geometry for single fuel form
1 - Right-cylindrical geometry for subfuel form or fuel pins and overall right-cylindrical for fuel block

(e) Heat-source-support computation option

-1 - Maximum support by ends
0 - Support by both end and radial portion
1 - Maximum support by radial portion

(f) End-insulation computation option

1 - Tradeoff end-insulation thickness against other generator components
0 - End-insulation thickness is fixed

(g) Insulation and heat-source-support option

0 - Solid-type insulation and support
1 - Foil- and honeycomb-type insulation and support

(h) Insulation and heat-source-support material option

0 - Treat insulation and heat-source support as independent components
1 - Assume insulation and heat source are same and calculate deflection of support material on the basis of total bearing area available.

(20) Transient Data Set

This block is repeated as many times as the user requires to simulate the transient operating profile of the RTG. The data sets must be sequenced in chronological order.

(21) Print Out Interval

Specification of this time interval controls the frequency of print-out of RTG data during a "dynamic" transient, e.g., start-up of RTG after fueling, transient operation during launch. This should not be less than 120 sec.

(22) Absolute Transient Factor

This factor specifies whether the present transient data set describes the "dynamic" transient condition (e.g., transient operation during launch) or a "static" condition (e.g., simple decay of radioisotope). If "dynamic", set equal to 1, if "static", set equal to 0.

(23) RTG Boundary Conditions

The RTG boundary temperature and radiator heat-transfer coefficient (convection and conduction) can be specified in order to permit simulation of changing RTG boundary conditions. An important transient condition requiring this option is the simulation of the RTG operation during launch. For example, the RTG may be exposed to the following launch profile: (1) RTG cooled by forced air flow with an ambient temperature T_1, (2) RTG dissipates heat to shroud by natural convection and radiation heat transfer with a boundary temperature T_2, and (3) shroud is removed and RTG dissipates heat solely by radiation heat transfer to an effective boundary temperature of T_3. In describing the above launch profile, the analyst may subdivide each of the above three phases of the launch into smaller time intervals by simply specifying the boundary temperature and the convection and conduction heat-transfer coefficient corresponding to each subinterval.

(24) Start-up Option

This option permits the analyst to study the transient performance of a given RTG design during start-up from a specified initial temperature.

APPENDIX B

SAMPLE TRANRTG OUTPUT

INPUT DATA
++++++++++

RADIATOR FIN INPUTS

RADIATOR MATERIAL I.D.	MAG-HM-1	NO. OF FINS	5.00
FIN EMISSIVITY	10.90	FIN LENGTH PARAMETER	6.1526
FIN THICKNESS PARAMETER	1.6516	FIN WEIGHT PARAMETER	0.405E-01

THERMOPILE INPUTS

THERMOELECTRIC MATERIAL	PBTE(2P-2N)	THERMOELECTRIC HARDWARE MATERIAL	SS304
THERMOELECTRIC HOT-SHOE MATERIAL	TUNGSTEN	THERMOELECTRIC COLD-SHOE MATERIAL	IRON-SNTE
THERMAL AND ELECTRICAL INSULATION MATERIAL	MICA	MODULE CLAD MATERIAL	NONE USED
ASSUMED ELEMENT LENGTH	1.40	CLOSED-CIRCUIT VOLTAGE PER COUPLE	0.0653
THERMOELECTRIC CURRENT	3.50	NO. OF MODULES	5.00
L/A FOR STAGE-1 N-ELEMENT	2.80	L/A FOR STAGE-1 P-ELEMENT	2.33
L/A FOR STAGE-2 N-ELEMENT	0.00	L/A FOR STAGE-2 P-ELEMENT	0.00
L/A FOR STAGE-3 N-ELEMENT	-0.00	L/A FOR STAGE-3 P-ELEMENT	-0.00
DENSITY FOR STAGE-1 OF N-ELEMENT	0.0179	DENSITY FOR STAGE-1 OF P-ELEMENT	0.0179
DENSITY FOR STAGE-2 OF N-ELEMENT	0.0000	DENSITY FOR STAGE-2 OF P-ELEMENT	0.0000
DENSITY FOR STAGE-3 OF N-ELEMENT	-0.0000	DENSITY FOR STAGE-3 OF P-ELEMENT	-0.0000
NO. OF SEGMENTS FOR T/E ELEMENTS	1.00	EVEN,1,OR EITHER,0,NO. OF ELEMENTS IN MODULE WIDTH	0.00
DENSITY OF HARDWARE RELATED TO THE T/E S	0.0176	DENSITY OF MODULE CLAD MATERIAL	0.0000
DENSITY OF T/E SHOE MATERIAL	0.0173	DENSITY OF INTER-ELEMENT INSULATION MATERIAL	0.0071
T/E HARDWARE THICKNESS FOR CONDUCTION MODE OF HT TRN	1.100	T/E HARDWARE THICKNESS FOR RADIATION MODE OF HT TRAN	0.000
RADIATION GAP BETWEEN HEAT SOURCE AND MODULE	0.000	THICKNESS OF T/E ELEMENT SHOES	0.127
MODULE CAN WALL THICKNESS	0.000	SEPARATION BETWEEN MODULE WALL AND GENERATOR INS.	0.025
THICKNESS OF INTER-ELEMENT INSULATION	0.113	EFFECTIVE THERMAL CONDUCTIVITY OF MODULE CAN WALL	0.0000
EFFECTIVE THERMAL CONDUCTIVITY OF INTER-ELEMENT INS	0.0050		

FUEL-FORM IMPACT CLAD INPUTS

FUEL-FORM CLAD MATERIAL	HASTELLOY C	INNER LINER CLAD MATERIAL	NONE USED

OUTER-SHELL CLAD MATERIAL	NONE USED	FUEL TUBE MATERIAL	MOLYBDENUM
TOUGHNESS PARAMETER FOR FUEL FORM CLAD	0.321E+04	THICKNESS OF CLAD INNER LINER	0.000
THICKNESS OF OUTER SHELL CLAD	0.000	THICKNESS OF FUEL TUBE	0.200
DENSITY OF FUEL FORM CLAD	0.0201	DENSITY OF CLAD INNER LINER	0.0000
DENSITY OF OUTER SHELL CLAD	0.0000	DENSITY OF FUEL TUBE	0.0195

FUEL-FORM INPUTS

FUEL FORM MATERIAL	PU-238 OXIDE	FUEL BLOCK MATERIAL	GRAPHITE
FUEL FORM POWER DENSITY	3.60	NORMALIZED MATRIX DENSITY FOR FUEL PIN ARRAY	00.60
FUEL PIN EFFECTIVENESS FACTOR	1.00	FUEL PIN ARRAY OPTION (0-CIRCLE,1-CLOSE PACK)	1.00
FUEL PIN TO FUEL TUBE SEPARATION	0.500	FUEL PIN SEPARATION	00.50
NO. OF FUEL PINS	10.00	EFFECTIVE SURFACE PWR. DENS. AVAILABLE FOR MODULE	10.00
HEAT TRANSFER TO MODULE (1-CONDUCTION,2-RADIATION)	1.00	DENSITY OF FUEL BLOCK	0.0198
DENSITY OF FUEL FORM	0.0251	DENSITY OF FUEL PIN	0.0251
LIMITING ASPECT RATIO FOR FUEL FORM	2.50	LIMITING ASPECT RATIO FOR FUEL PIN	4.00

HEAT SOURCE SUPPORT INPUTS

END HEAT SOURCE SUPPORT MATERIAL	MIN-K 2000	RADIAL HEAT SOURCE SUPPORT MATERIAL	MIN-K 2000
END THERMAL INSULATION MATERIAL	MIN-K 2000	RADIAL THERMAL INSULATION MATERIAL	MIN-K 2000
ABSOLUTE END SUPPORT (0-ALL END OR 1-SOME RADIAL)	1.00	ABSOLUTE RADIAL SUPPORT (0-ALL RADIAL OR 1-SOME END)	1.00
END SUPPORT ELASTIC MODULUS (COMPRESSION)	0.20E+04	RADIAL SUPPORT ELASTIC MODULUS (COMPRESSION)	0.20E+04
END SUPPORT ELASTIC MODULUS (SHEAR)	0.E+00	RADIAL SUPPORT ELASTIC MODULUS (SHEAR)	0.E+00
GEN LENGTH INDEPENDENT OF END DEFLECTION,0-NO,1-YES	1.00	END SUPPORT FOIL SEPARATION	0.000
RADIAL SUPPORT FOIL SEPARATION	0.000	END INSULATION FOIL SEPARATION	0.000
RADIAL INSULATION FOIL SEPARATION	0.000	END SUPPORT THERMAL CONDUCTIVITY	0.0008
RADIAL SUPPORT THERMAL CONDUCTIVITY	0.0008	END INSULATION THERMAL CONDUCTIVITY	0.0008
RADIAL INSULATION THERMAL CONDUCTIVITY	0.0008	END SUPPORT DENSITY	0.0009
RADIAL SUPPORT DENSITY	0.0009	END INSULATION DENSITY	0.0009
RADIAL INSULATION DENSITY	0.0009	MAX ALLOWED END SUPPORT DEFLECTION	0.0508

MAX ALLOWED RADIAL SUPPORT DEFLECTION	0.0508		
		GENERATOR SHELL INPUTS	
GENERATOR SHELL MATERIAL	MAGHM21A-T8	FINAL VALUE FOR GENERATOR LENGTH	300.00
NORMAL GENERATOR LENGTH INCREMENT	20.000	INITIAL VALUE FOR GENERATOR LENGTH	160.00
DENSITY OF GENERATOR SHELL	0.0639	THICKNESS OF END ABLATOR	0.000
RADIAL ABLATOR THICKNESS	0.000	THERMAL CONDUCTIVITY OF GENERATOR SHELL	1.370
LIMIT FOR GENERATOR ENVELOPE ASPECT RATIO	30.00	LIMIT FOR GENERATOR SHELL ASPECT RATIO	25.000
TOTAL HEAT DUMP CAPABILITY FOR ENDS (PERCENT)	0.500	GENERATOR SHELL THICKNESS	00.50
		RTG ANALYSIS COMPUTATION OPTIONS	
T/E ARRAY COMPUTATION SEQUENCE	1.00	GENERATOR LENGTH COMPUTATION SEQUENCE	1.00
T/E ELEMENT LENGTH COMPUTATION SEQUENCE	0.00	FUEL FORM GEOMETRY OPTION	1.000
HEAT SOURCE SUPPORT COMPUTATION OPTION	0.00	END INSULATION COMPUTATION OPTION	0.00
INSULATION AND HEAT SOURCE SUPPORT OPTION	0.00	INSULATION AND HEAT SOURCE SUPPORT MATERIAL OPTION	1.00
PRINT OPTION FOR OUTPUT DATA	0.00	PLOT OPTION	1.00
		TEMPERATURES	
T/E COLD JUNCTION TEMPERATURE	500.0	THERMAL INSULATION COLD SIDE TEMPERATURE	485.0
T/E HOT JUNCTION TEMPERATURE	800.0	THERMAL INSULATION HOT SIDE TEMPERATURE	813.0
HEAT SOURCE SURFACE TEMPERATURE	813.0	RADIATOR FIN AND GENERATOR SHELL TEMPERATURE	484.0
		GENERAL DESIGN INPUTS	
ASSUMED ENGINEERING EFFICIENCY	0.936	MIN ALLOWED T/E ELEMENT LENGTH	0.800
MAX ALLOWED T/E ELEMENT LENGTH	3.000	AXIAL G-LOAD	30.00
RADIAL G-LOAD	30.00	GENERATOR POWER LEVEL	250.0
HEAT SOURCE IMPACT VELOCITY	98.4	END OF MISSION T/E EFFICIENCY	0.0546

THE PRINT OUT ON THE FOLLOWING PAGE IS FOR THE MINIMUM WEIGHT GENERATOR WHICH COULD BE DESIGNED
BY THIS COMPUTER CODE WITH YOUR INPUT DATA

```
*WARNING*  HEAT SOURCE LENGTH EXCEEDS MODULE LENGTH BY MORE THAN ONE HEAT SOURCE DIAMETER

FOR LOW THERMAL CONDUCTIVITY HEAT SOURCES THE MODULE HEAT SOURCE MISMATCH MAY RESULT IN A LOWER
ENGINEERING EFFICIENCY THAN HAS BEEN CALCULATED HERE

HEAT SOURCE SURFACE TEMPERATURES MAY ALSO EXCEED DESIRED LIMITS
```

PAGE 1

SUMMARY OF OUTPUT DATA

GENERATOR LENGTH = 196.0

I GEOMETRIC DESIGN DATA	(CM)	(IN)
OVER ALL GENERATOR LENGTH	196.	77.2
RADIATOR FIN HEIGHT	19.3	7.6
DIAMETER OF GENERATOR SHELL (O.D.)	11.72	4.62
DIAMETER OF GENERATOR SHELL (I.D.)	10.72	4.22
BASE THICKNESS OF RADIATOR FIN	.304	0.120
DIAMETER OF HEAT SOURCE	5.72	2.25
DIAMETER OF FUEL BLOCK	5.72	2.25
LENGTH OF HEAT SOURCE	190.0	74.80
LENGTH OF SEGMENT OF HEAT SOURCE	3.80	1.50
DIAMETER OF FUEL PIN	1.18	00.47
DEPTH OF MODULE	1.654	0.651
WIDTH OF MODULE	3.2	1.26
LENGTH OF MODULE	80.97	31.88
LENGTH OF T/E ELEMENTS	1.400	0.551
NO. OF HEAT SOURCE SEGMENTS	50.	
NO. OF FUEL PINS	500.	
NO. OF T/E COUPLES IN GENERATOR	1094.	
NO. OF T/E COUPLES PER MODULE	220.	
NO. OF T/E ELEMENTS IN WIDTH OF MODULE	4.	

II COMPONENT WEIGHTS	(LB)	(KG)
TOTAL GENERATOR WEIGHT	189.2	85.9
HEAT SOURCE WEIGHT	104.0	47.2
MODULE WEIGHT	35.5	16.1
RADIATOR FIN WEIGHT	11.2	5.1
END HEAT SOURCE SUPPORT WEIGHT	00.12	00.05
RADIAL HEAT SOURCE SUPPORT WEIGHT	1.24	00.56
GENERATOR SHELL WEIGHT	13.82	6.28

III HEAT BALANCE AND THERMAL INVENTORY	(WATTS)
GENERATOR OUTPUT POWER (E)	250.0
GENERATOR INPUT POWER (TH)	4870.2
HEAT DUMPED BY RADIATOR (TH)	3374.0
HEAT DUMPED BY ENDS (TH)	30.2
GENERATOR ENGINEERING EFFICIENCY(DECIMAL)	0.940
T/E COUPLE EFFICIENCY (DECIMAL)	0.0546

OUTPUT DATA

GENERATOR LENGTH = 196.0

I GEOMETRIC DESIGN DATA

1 MODULE AND T/E

	(CM)	(IN)
DEPTH OF MODULE	1.654	0.651
WIDTH OF MODULE	3.20	1.26
LENGTH OF MODULE	80.97	31.88
T/E ELEMENT LENGTH	1.400	0.551
STAGE 1 LENGTH FOR SEGMENTED N-TYPE T/E ELEMENT	1.400	0.551
STAGE 1 LENGTH FOR SEGMENTED P-TYPE T/E ELEMENT	1.400	0.551
STAGE 2 LENGTH FOR SEGMENTED N-TYPE T/E ELEMENT	.000	0.000
STAGE 2 LENGTH FOR SEGMENTED P-TYPE T/E ELEMENT	.000	0.000
STAGE 3 LENGTH FOR SEGMENTED N-TYPE T/E ELEMENT	.000	0.000
STAGE 3 LENGTH FOR SEGMENTED P-TYPE T/E ELEMENT	.000	0.000
DEPTH OF N-TYPE ELEMENT	.645	0.254
DEPTH OF P-TYPE ELEMENT	.775	0.305
WIDTH OF N-TYPE ELEMENT	.775	0.305
WIDTH OF P-TYPE ELEMENT	.775	0.305
AREA OF MODULE PERPINDICULAR TO HEAT FLOW	259.3	40.2
HEAT LOSS AREA FOR MODULE ELECTRICAL AND THERMAL INSULATION	84.48	13.1
HEAT LOSS AREA FOR MODULE PERIPHERY	0.00	0.00
NO. OF T/E COUPLES IN GENERATOR	1394.	

NO. OF T/E COUPLES PER MODULE	220.	
T/E ELEMENT LENGTH ITERATION NO.	1.	
NO. OF COUPLES IN LENGTH OF MODULE	55.0	
NO. OF COUPLES IN WIDTH OF MODULE	4.0	

2 HEAT SOURCE AND FUEL FORM

	(CM)	(IN)
HEAT SOURCE DIAMETER	5.72	2.25
FUEL BLOCK DIAMETER	5.72	2.25
HEAT SOURCE LENGTH	190.0	74.8
HEAT SOURCE SEGMENT LENGTH	3.80	1.50
FUEL PIN CENTER TO CENTER SEPARATION	0.00	0.00
FUEL PIN DIAMETER	1.18	00.47
THICKNESS OF FUEL FORM CLAD	0.102	0.040
THICKNESS OF FUEL FORM CLAD LINER	0.000	0.000
THICKNESS OF FUEL FORM OVER-CLAD	0.000	0.000
THICKNESS OF FUEL TUBE	0.200	0.079
DIAMETER OF FUEL FORM	00.98	00.39
LENGTH OF FUEL FORM	179.8	70.8
NO. OF FUEL PINS	500.	
NO. OF CLAD ITERATIONS	10.	

OUTPUT DATA (CONTINUED)

GENERATOR LENGTH = 196.0

1 GEOMETRIC DESIGN DATA (CONTINUED)

2 HEAT SOURCE AND FUEL FORM (CONTINUED)	(CM)	(IN)
LENGTH OF FUEL FORM SEGMENT	3.6[illegible]	1.42
LENGTH INCREMENT TO SIZE FUEL FORM	[illegible].[illegible]3[illegible]	0.012
TOLERANCE ON LENGTH OF FUEL FORM	[illegible].[illegible]3[illegible]	0.012
FUEL FORM VOLUME	1352.8	82.5
FUEL PIN VOLUME	2.[illegible]	[illegible].16
RATIO OF FUEL FORM LENGTH TO DIAMETER	[illegible].[illegible]7	
NO. OF FUEL FORM SEGMENTS	5.	
FUEL FORM LENGTH ITERATION NO.	[illegible].	

3 RADIATOR FIN AND GENERATOR SHELL	(CM)	(IN)
OVER ALL GENERATOR LENGTH	196.[illegible]	77.2
RADIATOR FIN HEIGHT	19.26	7.58
RADIATOR FIN BASE THICKNESS	[illegible].3[illegible]4	0.120
OUTSIDE DIAMETER OF GENERATOR SHELL	11.72	4.62
INSIDE DIAMETER OF GENERATOR SHELL	1[illegible].72	4.22
NO. OF LARGE ITERATIONS FOR RADIATOR ANALYSIS	15.	
NO. OF SMALL ITERATIONS FOR RADIATOR ANALYSIS	1.	

4 INSULATION AND HEAT SOURCE SUPPORT	(CM)	(IN)
END SEPARATION BETWEEN HEAT SOURCE AND SHELL	2.501	0.984
RADIAL SEPARATION BETWEEN HEAT SOURCE AND SHELL	2.500	0.984
HEAT SOURCE DEFLECTION AGAINST END SUPPORT	0.152	0.060
HEAT SOURCE DEFLECTION AGAINST RADIAL SUPPORT	0.018	0.007
HEAT LOSS AREA FOR RADIAL INSULATION	675.8	104.8
HEAT LOSS AREA FOR END INSULATION	0.00	0.00
END AREA AVAILABLE FOR SUPPORT	25.7	4.0
AREA REQUIRED FOR END SUPPORT	76.8	11.9
RADIAL AREA AVAILABLE FOR SUPPORT	1059.7	164.3
RADIAL AREA REQUIRED FOR SUPPORT	383.8	59.5
HEAT LOSS AREA FOR END HEAT SOURCE SUPPORT	25.7	4.0
HEAT LOSS AREA FOR RADIAL HEAT SOURCE SUPPORT	383.8	59.5
NO. OF END INSULATION ITERATIONS	1.0	

PAGE 4

OUTPUT DATA(CONTINUED)
=====================

GENERATOR LENGTH = 196.0

II COMPONENT WEIGHTS	(LB)	(KG)
TOTAL GENERATOR WEIGHT	189.19	85.89
1 MODULE AND T/E		
WEIGHT OF T/E MATERIALS	35.46	16.10
WEIGHT OF T/E HARDWARE	19.30	8.76
WEIGHT OF MODULE CAN	0. 0	0.00
WEIGHT OF T/E MODULE	35.46	16.10
2 HEAT SOURCE AND FUEL FORM		
FUEL FORM WEIGHT	33.96	15.42
FUEL FORM SEGMENT WEIGHT	00.69	00.31
FUEL PIN WEIGHT	00.07	00.03
CLAD FUEL PIN WEIGHT	00.10	00.04
FUEL TUBE WEIGHT	12.86	5.94
FUEL BLOCK WEIGHT	42.40	19.29
WEIGHT OF CLAD LINER	0. 0	0.00
WEIGHT OF OUTER CLAD	0. 0	0.00
PRIMARY CLAD WEIGHT	14.70	6.67
WEIGHT OF REENTRY ABLATOR	0. 0	0.00
HEAT SOURCE TOTAL WEIGHT	[illegible]	47.21

	(LB)	(KG)
3 RADIATOR FIN AND GENERATOR SHELL		
RADIATOR FIN WEIGHT	11.24	5.10
GENERATOR SHELL WEIGHT	13.82	6.28
4 INSULATION AND HEAT SOURCE SUPPORT		
END INSULATION WEIGHT	00.29	00.13
RADIAL INSULATION WEIGHT	3.72	1.69
END HEAT SOURCE SUPPORT WEIGHT	00.12	00.05
RADIAL HEAT SOURCE SUPPORT WEIGHT	1.24	00.56

III HEAT BALANCE AND THERMAL INVENTORY

	(WATTS)		(WATTS)
1 MODULE AND T/E		HEAT LOSS THROUGH END HEAT SOURCE SUPPORT	5.40
T/E COUPLE EFFICIENCY (1)	.0546	HEAT LOSS THROUGH RADIAL HEAT SOURCE SUPPORT	56.15
HEAT LOSS THROUGH MODULE CAN	7.60	TOTAL PARASITIC HEAT LOSS	289.33
HEAT LOSS THROUGH ELECTRICAL INSULATION	76.62		
SURFACE POWER DENSITY (2)	3.05	**5 GENERAL**	
2 HEAT SOURCE AND FUEL FORM		CALCULATED ENGINEERING EFFICIENCY (1)	0.0485
HEAT SOURCE THERMAL INVENTORY	487[illegible].21	GENERATOR POWER LEVEL	250.00
FUEL FORM POWER DENSITY (3)	3.6060		
3 RADIATOR FIN AND GENERATOR SHELL			
HEAT DUMPED BY RADIATOR FINS	3373.09		
HEAT DUMPED BY GENERATOR SHELL ENDS	3[illegible].22		
4 INSULATION AND HEAT SOURCE SUPPORT			
HEAT LOSS THROUGH END INSULATION	6.78		
HEAT LOSS THROUGH RADIAL INSULATION	98.49		
HEAT LOSS THROUGH MODULE WEDGE INSULATION	[illegible].77		
HEAT LOSS BY RADIATION FROM MODULE PERIPHERY	45.52		

(1) DECIMAL UNITS
(2) WATTS (TH) PER SQ. CM.
(3) WATTS (TH) PER CUBIC CM.

1	97	12	1	160.[illegible]	133.6721
11	96	12	2	180.[illegible]	130.0459
21	95	12	3	220.[illegible]	189.5643
31	96	12	4	220.[illegible]	191.8135
[illegible]	96	12	5	216.[illegible]	191.2577
26	96	12	6	212.[illegible]	190.74[illegible]
24	95	12	7	208.[illegible]	190.3355
[illegible]	95	12	8	204.[illegible]	189.8841
21	95	12	9	200.[illegible]	189.554
[illegible]	95	12	10	196.[illegible]	189.1771
[illegible]	96	12	11	192.[illegible]	190.29[illegible]
18	95	12	12	196.[illegible]	189.18[illegible]

GENERATOR AND COMPONENT WEIGHTS VS. GENERATOR LENGTH
WEIGHT IN LBS
TOTAL=+, HT SOURCE=*, RAD FIN=O, RAD SHELL=., STR SUPPORT + INS=X

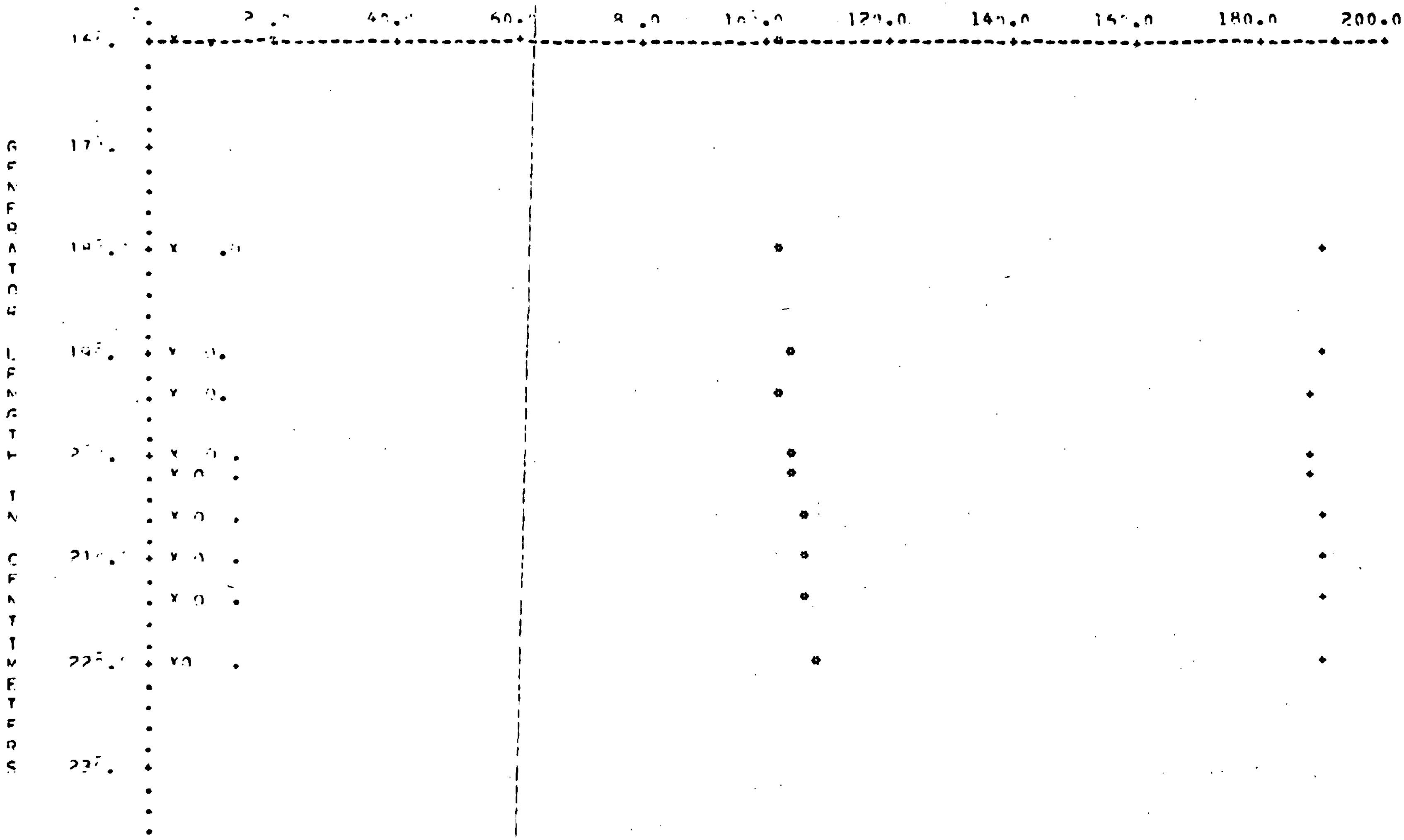

ELAPSED TIME (HOURS)	BOUNDRY TEMP. (KELVIN)	RAD. H.T. COEF (CAL/SEC K SQCM.)
0.5000E+04	0.5000E+01	0.E+00

POWER(CPL) (WATTS)	EFFICIENCY(CPL) (DEC.PERCENT)	POWER(RTG) (WATTS)	EFFICIENCY(RTG) (DEC.PERCENT)	SPECIFIC PWR (DECIMAL)	NORM. POWER (DECIMAL)	INT. RESIS. (OHMS)	CURRENT (AMPS)
0.228	0.055	256.115	0.046	1.329	1.000	24.784	3.445

TEMP DIST NLEG (KELVIN)	SEEBECK C.NLEG (MICROVOLTS/K)	TEMP DIST PLEG (KELVIN)	SEEBECK C.PLEG (MICRVOLTS/K)
0.7988E+03	0.2451E-03	0.7988E+03	0.2818E-03
0.7838E+03	0.2474E-03	0.7838E+03	0.2800E-03
0.7689E+03	0.2492E-03	0.7689E+03	0.2782E-03
0.7539E+03	0.2505E-03	0.7539E+03	0.2760E-03
0.7390E+03	0.2512E-03	0.7390E+03	0.2731E-03
0.7240E+03	0.2514E-03	0.7240E+03	0.2697E-03
0.7091E+03	0.2510E-03	0.7091E+03	0.2655E-03
0.6941E+03	0.2500E-03	0.6941E+03	0.2607E-03
0.6792E+03	0.2484E-03	0.6792E+03	0.2552E-03
0.6642E+03	0.2461E-03	0.6642E+03	0.2491E-03
0.6493E+03	0.2433E-03	0.6493E+03	0.2425E-03
0.6493E+03	0.2433E-03	0.6493E+03	0.2425E-03
0.6343E+03	0.2397E-03	0.6343E+03	0.2355E-03
0.6194E+03	0.2356E-03	0.6194E+03	0.2282E-03
0.6044E+03	0.2309E-03	0.6044E+03	0.2205E-03
0.5895E+03	0.2256E-03	0.5895E+03	0.2127E-03
0.5745E+03	0.2199E-03	0.5745E+03	0.2046E-03
0.5596E+03	0.2138E-03	0.5596E+03	0.1963E-03
0.5446E+03	0.2074E-03	0.5446E+03	0.1879E-03
0.5297E+03	0.2007E-03	0.5297E+03	0.1794E-03
0.5147E+03	0.1938E-03	0.5147E+03	0.1707E-03

TEMP DIST NLEG (KELVIN)	RESISTVTY NLEG (MICROOHM-CM)	THERM COND NLEG (WATTS/CM-K)	TEMP DIST PLEG (KELVIN)	RESISTVTY PLEG (MICROOHM-CM)	THERM COND PLEG (WATTS/CM-K)
0.7913E+03	0.6511E-02	0.1700E-01	0.7913E+03	0.5398E-02	0.1115E-01
0.7763E+03	0.6350E-02	0.1659E-01	0.7763E+03	0.5232E-02	0.1099E-01
0.7614E+03	0.6188E-02	0.1615E-01	0.7614E+03	0.5065E-02	0.1088E-01
0.7464E+03	0.6020E-02	0.1573E-01	0.7464E+03	0.4890E-02	0.1082E-01
0.7315E+03	0.5844E-02	0.1536E-01	0.7315E+03	0.4703E-02	0.1081E-01
0.7165E+03	0.5659E-02	0.1507E-01	0.7165E+03	0.4503E-02	0.1085E-01
0.7016E+03	0.5463E-02	0.1484E-01	0.7016E+03	0.4292E-02	0.1094E-01
0.6866E+03	0.5258E-02	0.1470E-01	0.6866E+03	0.4071E-02	0.1106E-01
0.6717E+03	0.5045E-02	0.1463E-01	0.6717E+03	0.3843E-02	0.1120E-01
0.6567E+03	0.4824E-02	0.1462E-01	0.6567E+03	0.3612E-02	0.1137E-01
0.6418E+03	0.4597E-02	0.1466E-01	0.6418E+03	0.3380E-02	0.1156E-01
0.6268E+03	0.4367E-02	0.1475E-01	0.6268E+03	0.3151E-02	0.1179E-01
0.6119E+03	0.4133E-02	0.1487E-01	0.6119E+03	0.2927E-02	0.1206E-01
0.5969E+03	0.3897E-02	0.1503E-01	0.5969E+03	0.2711E-02	0.1238E-01
0.5820E+03	0.3661E-02	0.1521E-01	0.5820E+03	0.2504E-02	0.1276E-01
0.5670E+03	0.3425E-02	0.1543E-01	0.5670E+03	0.2308E-02	0.1322E-01
0.5521E+03	0.3191E-02	0.1566E-01	0.5521E+03	0.2123E-02	0.1377E-01
0.5371E+03	0.2959E-02	0.1593E-01	0.5371E+03	0.1950E-02	0.1442E-01
0.5222E+03	0.2731E-02	0.1624E-01	0.5222E+03	0.1788E-02	0.1517E-01
0.5072E+03	0.2507E-02	0.1658E-01	0.5072E+03	0.1638E-02	0.1603E-01

TEMP DIST(N,P) (KELVIN)	SECT.LENGTH(N,P) (CENTIMETERS)	EL.WIDTH(N,P) (CENTIMETERS)	EL.DEPTH(N,P) (CENTIMETERS)	EL.DIAM. (N,P) (CENTIMETERS)
0.7913E+03	0.8820E-01	0.7746E+00	0.6455E+00	0.7979E+00
0.7763E+03	0.8494E-01	0.7746E+00	0.6455E+00	0.7979E+00
0.7614E+03	0.8153E-01	0.7746E+00	0.6455E+00	0.7979E+00
0.7464E+03	0.7827E-01	0.7746E+00	0.6455E+00	0.7979E+00
0.7315E+03	0.7532E-01	0.7746E+00	0.6455E+00	0.7979E+00
0.7165E+03	0.7276E-01	0.7746E+00	0.6455E+00	0.7979E+00
0.7016E+03	0.7061E-01	0.7746E+00	0.6455E+00	0.7979E+00
0.6866E+03	0.6885E-01	0.7746E+00	0.6455E+00	0.7979E+00
0.6717E+03	0.6744E-01	0.7746E+00	0.6455E+00	0.7979E+00
0.6567E+03	0.6632E-01	0.7746E+00	0.6455E+00	0.7979E+00
0.6418E+03	0.6546E-01	0.7746E+00	0.6455E+00	0.7979E+00
0.6268E+03	0.6508E-01	0.7746E+00	0.6455E+00	0.7979E+00
0.6119E+03	0.6461E-01	0.7746E+00	0.6455E+00	0.7979E+00
0.5969E+03	0.6428E-01	0.7746E+00	0.6455E+00	0.7979E+00
0.5820E+03	0.6405E-01	0.7746E+00	0.6455E+00	0.7979E+00
0.5670E+03	0.6394E-01	0.7746E+00	0.6455E+00	0.7979E+00
0.5521E+03	0.6395E-01	0.7746E+00	0.6455E+00	0.7979E+00
0.5371E+03	0.6408E-01	0.7746E+00	0.6455E+00	0.7979E+00
0.5222E+03	0.6436E-01	0.7746E+00	0.6455E+00	0.7979E+00
0.5072E+03	0.6481E-01	0.7746E+00	0.6455E+00	0.7979E+00
0.7913E+03	0.7803E-01	0.7746E+00	0.7746E+00	0.8740E+00
0.7763E+03	0.7533E-01	0.7746E+00	0.7746E+00	0.8740E+00
0.7614E+03	0.7303E-01	0.7746E+00	0.7746E+00	0.8740E+00
0.7464E+03	0.7116E-01	0.7746E+00	0.7746E+00	0.8740E+00
0.7315E+03	0.6967E-01	0.7746E+00	0.7746E+00	0.8740E+00
0.7165E+03	0.6850E-01	0.7746E+00	0.7746E+00	0.8740E+00
0.7016E+03	0.6760E-01	0.7746E+00	0.7746E+00	0.8740E+00
0.6866E+03	0.6689E-01	0.7746E+00	0.7746E+00	0.8740E+00
0.6717E+03	0.6635E-01	0.7746E+00	0.7746E+00	0.8740E+00
0.6567E+03	0.6596E-01	0.7746E+00	0.7746E+00	0.8740E+00
0.6418E+03	0.6572E-01	0.7746E+00	0.7746E+00	0.8740E+00
0.6268E+03	0.6630E-01	0.7746E+00	0.7746E+00	0.8740E+00
0.6119E+03	0.6649E-01	0.7746E+00	0.7746E+00	0.8740E+00
0.5969E+03	0.6696E-01	0.7746E+00	0.7746E+00	0.8740E+00
0.5820E+03	0.6777E-01	0.7746E+00	0.7746E+00	0.8740E+00
0.5670E+03	0.6898E-01	0.7746E+00	0.7746E+00	0.8740E+00
0.5521E+03	0.7064E-01	0.7746E+00	0.7746E+00	0.8740E+00
0.5371E+03	0.7276E-01	0.7746E+00	0.7746E+00	0.8740E+00
0.5222E+03	0.7536E-01	0.7746E+00	0.7746E+00	0.8740E+00
0.5072E+03	0.7840E-01	0.7746E+00	0.7746E+00	0.8740E+00

NODE	TEMP(K)	NODE	TEMP(K)	NODE	TEMP(K)	NODE	TEMP(K)
1	813.5	11	476.4	21	695.5	31	544.2
2	813.9	12	476.4	22	679.6	32	530.7
3	813.9	13	796.1	23	663.7	33	517.7
4	594.0	14	498.9	24	647.9	34	505.1
5	529.8	15	788.7	25	632.3	35	480.2
6	594.0	16	773.7	26	616.8	36	430.2
7	494.0	17	758.5	27	601.7	37	359.8
8	480.9	18	743.1	28	586.8	38	306.8
9	476.9	19	727.4	29	572.2	39	*000.0
10	477.0	20	711.5	30	558.0	40	-0.0

647.5 647.5 0.8 0.7

0.100E+01 0.100E+01 0.281E-03 0.246E-03

0.537E-02	0.520E-02	0.504E-02	0.486E-02	0.467E-02	0.447E-02	0.426E-02
0.404E-02	0.381E-02	0.358E-02	0.335E-02	0.313E-02	0.290E-02	0.269E-02
0.249E-02	0.229E-02	0.211E-02	0.194E-02	0.178E-02	0.163E-02	0.648E-02
0.632E-02	0.616E-02	0.599E-02	0.582E-02	0.563E-02	0.544E-02	0.523E-02
0.502E-02	0.480E-02	0.457E-02	0.434E-02	0.411E-02	0.387E-02	0.364E-02
0.341E-02	0.317E-02	0.294E-02	0.272E-02	0.249E-02	0.201E-03	0.E+00
0.E+00	0.E+00	0.E+00	0.E+00	0.E+00	0.E+00	0.E+00
0.E+00	0.E+00	0.E+00	0.E+00	0.E+00	0.E+00	0.E+00
0.E+00	0.E+00	0.E+00	0.E+00	0.763E-04	0.E+00	0.E+00
0.E+00	0.E+00	0.E+00	0.E+00	0.E+00	0.E+00	0.E+00
0.E+00	0.E+00	0.E+00	0.E+00	0.E+00	0.E+00	0.E+00
0.E+00	0.E+00	0.E+00	0.281E-03	0.280E-03	0.278E-03	0.276E-03
0.273E-03	0.269E-03	0.265E-03	0.260E-03	0.254E-03	0.248E-03	0.242E-03
0.242E-03	0.235E-03	0.227E-03	0.220E-03	0.212E-03	0.204E-03	0.196E-03
0.187E-03	0.179E-03	0.246E-03	0.248E-03	0.249E-03	0.251E-03	0.251E-03
0.251E-03	0.251E-03	0.250E-03	0.248E-03	0.246E-03	0.243E-03	0.243E-03
0.239E-03	0.235E-03	0.230E-03	0.225E-03	0.219E-03	0.213E-03	0.207E-03
0.200E-03	0.169E-01	0.165E-01	0.161E-01	0.157E-01	0.153E-01	0.150E-01
0.148E-01	0.147E-01	0.146E-01	0.146E-01	0.147E-01	0.148E-01	0.149E-01
0.150E-01	0.152E-01	0.154E-01	0.157E-01	0.160E-01	0.163E-01	0.166E-01
0.111E-01	0.110E-01	0.109E-01	0.108E-01	0.108E-01	0.109E-01	0.110E-01
0.111E-01	0.112E-01	0.114E-01	0.116E-01	0.118E-01	0.121E-01	0.124E-01
0.128E-01	0.133E-01	0.138E-01	0.145E-01	0.152E-01	0.161E-01	0.100E+00

0.116-127	0.658E+29	0.149E+02	0.157-124	0.882E-01	0.780E-01	0.500E+00
0.600E+00	0.796E+03	0.140E+01	0.140E+01	0.500E-01	0.200E-03	0.438E-04
0.657E-05	0.200E+02	0.200E+02	0.192E-01	0.499E+03	0.193E-03	0.170E-03

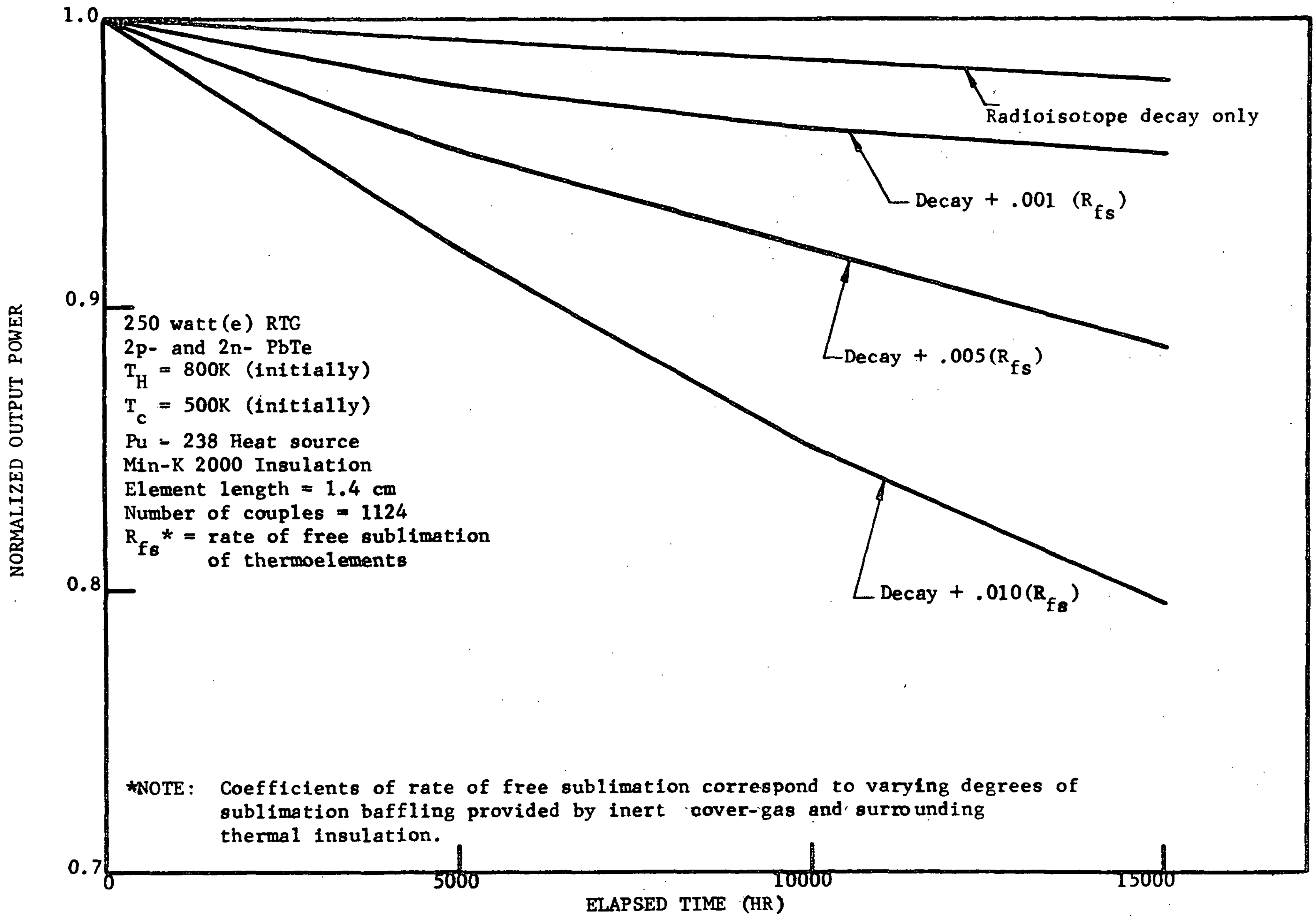

FIGURE B-1. CALCULATED RTG NORMALIZED POWER VERSUS TIMF